ÇUKUROVA UNIVERSITY
INSTITUTE OF NATURAL AND APPLIED SCIENCES

MSc. THESIS

Merve İNCE

ANALYSES OF HB, HE, HO AND HF CALORIMETERS OF CMS DETECTOR WITH 2015 COSMIC DATA AND PROTON - PROTON COLLISION DATA AT Ös = 13 TeV

DEPARTMENT OF PHYSICS

ADANA, 2016

ÇUKUROVA UNIVERSITY
INSTITUTE OF NATURAL AND APPLIED SCIENCES

ANALYSES OF HB, HE, HO AND HF CALORIMETERS OF CMS DETECTOR WITH 2015 COSMIC DATA AND PROTON – PROTON COLLISIONS AT $\sqrt{s}$ = 13 TeV

Merve İNCE

MSc THESIS

DEPARTMENT OF PHYSICS

We certify that the thesis titled above was reviewed and approved for the award of degree of the Master of Science by the board of jury on 22 /07/2016.

…………………………...	………………………………….…	…………...……………..……
Prof. Dr. İsa DUMANOĞLU	Prof. Dr. Aysel KAYIŞ TOPAKSU	Assoc.Prof.Dr. Bayram TALİ
SUPERVISOR	MEMBER	MEMBER

This MSc Thesis is performed in Department of Physics of Institute of Natural And Applied Sciences of Çukurova University.
Registration Number:

Prof. Dr. Mustafa GÖK
Director
Institute of Natural and Applied Sciences

This Study was supported by Çukurova University Scientific Research Fund.
Project Number: FYL-2015-4661

To my parents

ABSTRACT

MSc. THESIS

ANALYSES OF HB, HE, HO AND HF CALORIMETERS OF CMS DETECTOR WITH 2015 COSMIC DATA AND PROTON – PROTON COLLISION DATA AT √s = 13 TeV

Merve İNCE

ÇUKUROVA UNIVERSITY
INSTITUTE OF NATURAL AND APPLIED SCIENCES
DEPARTMENT OF PHYSICS

Supervisor : Prof. Dr. İsa DUMANOĞLU
Year: 2016, Page: 73
Jury : Prof. Dr. İsa DUMANOĞLU
: Prof. Dr. Aysel KAYIŞ TOPAKSU
: Assoc. Prof. Dr. Bayram TALİ

In 2015, the CMS detector took cosmic muon and proton-proton collision data at $\sqrt{s}$ = 13 TeV. General performance, such as energy and time structure of the HCAL which is one of the sub-detectors of the CMS was controlled with those data. The HCAL should have a good energy and time resolution. So, energy and time distributions of all sub-systems (HB, HE, HO, HF) of HCAL should be controlled regularly. One of the methods used to do these controls is, to benefit from the cosmic ray muon data which is recorded when there is no collision in the detector. The CMS detector is constantly exposed to cosmic muon rays which come from outer space. Cosmic muon rays hit various part of the CMS detector and create signals in the various sub-systems of CMS. So, these data allow to test and calibrate all detector components. The response of the CMS detector to cosmic muons was measured using cosmic muon data (MWGR, CRUZET and CRAFT) which were taken at different time periods. Before the collision data, Beam Splash data were also taken. During beam splash data taking, the CMS detector is exposed to dense particle flow and the response of each sub-system of the detector is investigated. Beam Splash data are very important for performance information of the sub-systems of the HCAL. The CMS detector was prepared for the collision data with the beam splash data. After the two-year technical stop the CMS detector started to take proton-proton collision data at a center of mass energy of $\sqrt{s}$ = 13 TeV. The performance analysis studies of the CMS detector were also performed using this collision data. In this thesis general performance analysis of HCAL systems was carried out using cosmic muon and proton-proton collision data.

Key Words: HCAL, Cosmic Muon, Beam Splash, Collision Data

ÖZ

YÜKSEK LİSANS TEZİ

CMS DETEKTÖRÜNÜN HB, HE, HO VE HF KALORİMETRELERİNİN 2015 KOZMİK VERİ VE √s = 13 TeV PROTON – PROTON ÇARPIŞMA VERİSİ İLE ANALİZİ

Merve İNCE

ÇUKUROVA ÜNİVERSİTESİ
FEN BİLİMLERİ ENSTİTÜSÜ
FİZİK ANABİLİM DALI

Danışman : Prof. Dr. İsa DUMANOĞLU
Yıl: 2016, Sayfa: 73
Jüri : Prof. Dr. İsa DUMANOĞLU
: Prof. Dr. Aysel KAYIŞ TOPAKSU
: Doç. Dr. Bayram TALİ

2015 yılında CMS detektörü kozmik muon ve √s = 13 TeV'de proton-proton çarpışma verileri almıştır. Bu veriler ile CMS detektörünün alt detektörlerinden biri olan HKAL'in genel performansı (enerji ve zaman yapısı) kontrol edilmiştir. HKAL iyi bir enerji ve zaman çözünürlüğüne sahip olmalıdır. Bundan dolayı HKAL'in bütün sistemlerinin (HB, HE, HO, HF) enerji ve zaman değerleri düzenli olarak kontrol edilmelidir. Bu kontrollerin yapılması için kullanılan yöntemlerden biri, detektörde çarpışma olmadığı zaman kaydedilen kozmik muon ışın verilerinden yararlanmaktır. CMS detektörü uzaydan gelen kozmik muon ışınlarına maruz kalmaktadır. Kozmik muon ışınları CMS detektörünün çeşitli yerlerine çarparak sinyaller üretmektedir. Bundan dolayı, bu veriler detektörün tüm elemanlarının kalibrasyonuna ve testine olanak sağlar. CMS detektörünün kozmik verilere olan tepkisi değişik zaman dilimlerinde alınan kozmik muon (MWGR, CRUZET ve CRAFT) verileri ile ölçülmüştür. Çarpışma verileri alımından önceki periyotta ise Beam splash verileri alınmıştır. CMS detektörü yoğun parçacık akısına maruz bırakılmıştır ve detektörün her bir alt sisteminin tepkisi incelenmiştir. Beam splash verileri HKAL'in alt sistemlerinin performans bilgisi için önemlidir. Beam splash verileri ile CMS detektörü çarpışma verilerine hazırlanmıştır. İki yıllık teknik bir aradan sonra CMS detektörü kütle merkezi enerjisi √s = 13 TeV 'de proton-proton çarpışma verileri almıştır. Bu çarpışmadan alınan verilerle CMS detektörünün performans analiz çalışmaları yürütülmüştür. Bu çalışmada, kozmik muon ve proton-proton çarpışma verileri ile HKAL sisteminin genel performans analizi üzerine çalışılmıştır.

Anahtar Kelimeler: HKAL, Kozmik Muon, Beam Splash, Çarpışma Verileri

ACKNOWLEDGMENTS

I would like to express my gratitude to my supervisor Prof. Dr. İsa DUMANOĞLU for his excellent guidance, motivation and encouragement during my MSc studies. He always supported me in the best way. It was great pleasure for me to be his student.

I would like to thank Cukurova University High Energy Physics groups members, Prof. Dr. Gülsen ÖNENGÜT, Prof. Dr. Eda EŞKUT, Prof. Dr. Ayşe POLATÖZ and Prof. Dr. Aysel KAYIŞ TOPAKSU for their contributions and help.

I owe a great debt of gratitude to Dr. Emine GÜRPINAR, Yalçın GÜLER and Assoc. Prof. Dr. Bayram TALİ for their interest, support and guidance throughout my thesis work. Also, I would like to give special thanks to Assoc. Prof. Dr. Shuichi KUNORI for his interest and help.

I wish to thank my friends and colleagues Zuhal Şeyma DEMİROĞLU, Furkan DÖLEK and Ümit SÖZBİLİR for sharing their suggestions and support during the writing of this theis.

I would like to extend my deepest gratitude to my dear father, my mother and my sister for their encouragement and support throughout my life. I always feel their love. Last, but not least, thanks are due to my dear fiance and best friend Samet LEZKİ for sharing this tiring journey with me. Thank you Samet for being in my life, your love, your wonderful care, encouragement and support.

I wish to thank my High Energy Physics friends for their friendship during the time I was at CERN.

Special thanks are to TAEK who sponsored me during the time I have spent at CERN.

CONTENTS **PAGE**

LIST OF TABLES **PAGE**

LIST OF FIGURES **PAGE**

ABBREVIATIONS

SM	: Standard Model
SUSY	: Super Symmetry
MSSM	: Minimal Supersymmetric Standard Model
CERN	: Conceil Europeenne pour la Recherche Nucleaire
FERMILAB	: Fermi National Accelerator Laboratory
DESY	: Deutsches Elektronen-Synchrotron
SLAC	: Stanford Linear Accelerator Center
EM	: Electromagnetic
QCD	: Quantum Chromo Dynamics
QED	: Quantum Electro Dynamics
LHC	: Large Hadron Collider
ATLAS	: A Toroidal LHC Apparatus
CMS	: Compact Muon Solenoid
ALICE	: A Large Ion Collider
LHCb	: Large Hadron Collider beauty
LHCf	: Large Hadron Collider forward
TOTEM	: TOTal Elastic and Diffractive Cross Section Measurement
LEP	: Large Electron Positron
LINAC2	: Linear Accelerator
PSB	: Proton Synchrotron Booster
PS	: Proton Synchrotron
SPS	: Super Proton Synchrotron
TIB	: Tracker Inner Barrel
TOB	: Tracker Outer Barrel
TID	: Tracker Inner Disk
TEC	: Tracker End Caps
CASTOR	: Centauro And Strange Object Research
ZDC	: Zero Degree Calorimeter
ECAL	: Electromagnetic Calorimeter

EB	: Electromagnetic Barrel
EE	: Electromagnetic Endcap
ES	: Electromagnetic Preshower
HCAL	: Hadronic Calorimeter
HB	: Hadronic Barrel
HE	: Hadronic Endcap
HO	: Hadronic Outer
HF	: Hadronic Forward
DT	: Drift Tubes
CSC	: Cathode Strip Chambers
RPC	: Resistive Plate Chambers
L1	: Level-1
HLT	: High Level Trigger
APD	: Avalanche Photo Diode
SC	: Super Cyristal
VPT	: Vacuum Photo Triode
WLS	: Wavelength Shifting Fiber
HPD	: Hybrid Photo Diode
PMT	: Photo Multiplier Tube
MWGR	: Mid-Week Global Run
CRUZET	: Cosmic Run at Zero Tesla
CRAFT	: Cosmic Run at Four Tesla
QIE	: Charge Integrator
η	: Pseudorapidity
θ	: Polar Angle
φ	: Azimuthal Angle
PbWO_4	: Lead Tungstate
MeV	: Million Electron Volt
GeV	: Billion Electron Volt
TeV	:Trillion Electron Volt
L	: Luminosity

ns	: Nano Second
T	: Tesla
GJ	: Giga Joule
MHz	: MegaHertz
kHz	: kiloHertz
$\sqrt{s}$	: Center of Mass Energy
λ_1	: Interaction Length
X_0	: Radiation Length
P_T	: Transverse Momentum
E_T	: Transverse Energy
Pb	: Lead
Au	: Gold
Cu	: Copper
Zn	: Zinc
Ar	: Argon
CO_2	: Carbone Dioxide

1. INTRODUCTION

High energy physics or particle physics is the science that investigates the structures of the subatomic particles and the interactions between these particles. During the historical development, humans tried to find answers to some questions such as what are the basic constituents of matter that creates the universe or what are the interactions which hold them? Empedocles had an idea that all things are made of four fundamental components: air, water, soil and fire. They interact with each other in various ways. From the Empedocles's idea in B.C. 400s, there has been a lot of effort to solve this problem. This idea has survived many centuries until particle physicists started to find answers to these kinds of questions. Now, in particle physics there are some theoretical models such as Standard Model (SM), super symmetry (SUSY), string theory, etc., whose aspects need to be confirmed by experiments. There are experimental centers in the world to do particle physics experiments such as; Conseil Européen pour la Recherche Nucléaire (CERN), Fermi National Accelerator Laboratory (FERMILAB), Deutsches Elektronen-Synchrotron (DESY), Stanford Linear Accelerator Center (SLAC), etc.

The SM, known as the best model of the modern particle physics, is a very successful model which identifies the basic constituents of matter. The SM tries to clarify how matter behaves and interacts in very high energies by investigating fundamental particles known as fermions, anti-fermions and mediating bosons. The quarks and leptons which are the basic constituents of matter according to SM belong to the fermion family. The fermions are particles which have half integer spin and obey the Pauli Exclusion Principle and are described by the Fermi-Dirac statistics. The photon, $W^{\pm}$, Z^{0} and gluons are called as gauge bosons, they have integer spin and are described by the Bose-Einstein statistics and don't obey the Pauli Exclusion Principle. The Higgs is a scalar particle and has spin 0. So the SM has six leptons and six quarks, twelve gauge bosons (eight gluons, photon, $W^{\pm}$, Z^{0}) and one Higgs particle. Particle interactions are described by four basic forces: electromagnetic, weak, strong and gravitational. Gravity is the only one the SM doesn't explain. (http://home.cern/about/physics/standard-model).

The leptons are fundamental particles which don't participate in strong interactions. There are six leptons grouped into three lepton families: electron (e), muon (μ) and tau (τ) with a charge of -1.6×10^{-19} C ($-e$) and their neutrinos: electron neutrino (ν_e), muon neutrino (ν_μ) and tau neutrino (ν_τ) with zero charge. According to SM, neutrinos should have zero masses, but some experimental results from neutrino experiments have indicated that neutrinos have nonzero mass. All leptons have their antiparticles called as anti-leptons. All features of the antileptons are (except their charges for charged leptons and few quantum numbers) the same with the leptons. The best-known member of the lepton family is the electron that was discovered by Thomson in 1897. Electron is a fundamental particle that has half integer spin. The antiparticle of the electron is the positron (e^+) and its mass and spin are identical with the electron but it has positive electrical charge (1.6×10^{-19} C = e). The charge of the muon and tau lepton is equal to the charge of the electron. The properties of leptons are given in the Table 1.1. The charged leptons interact via both EM and weak forces, while uncharged leptons (neutrinos) only interact via weak force.

Table 1.1. Properties of leptons.

Name	Symbol	Charge (e)	Mass (GeV/c^2)
electron	e	-1	0.511
electron neutrino	ν_e	0	0
muon	μ	-1	105.7
muon neutrino	ν_μ	0	0
tau	τ	-1	1784
tau neutrino	ν_τ	0	0

The quarks which have six flavors are also known as fundamental particles and carry half integer spin like leptons. They are grouped into three quark families: up (u) and down (d), charm (c) and strange (s), top (t) and bottom (b). The u, c, t quarks have electric charge $2e/3$, while d, s, b quarks have electric charge $-e/3$. The symbols, masses and charges of the quarks are given in Table 1.2. As leptons, each quark has also its own antiquark. The antiquarks have the same mass and spin with quarks; electric charges of antiquarks are opposite to that of the quarks. They are indicated by adding a bar on the quark symbols. u, c, t quarks have their antiquarks as $\bar{u}$, $\bar{c}$, $\bar{t}$ with a charge of $-2e/3$ and d, s, b quarks as $\bar{d}$, $\bar{s}$, $\bar{b}$ with a charge of $e/3$ (K.A. Olive et al.).

Table 1.2. Properties of quarks.

Name	Symbol	Charge (e)	Mass (GeV/c^2)
up quark	u	$2e/3$	2.4×10^{-3}
down quark	d	$-e/3$	4.8×10^{-3}
strange quark	s	$-e/3$	0.1
charm quark	c	$2e/3$	1.27
bottom quark	b	$-e/3$	4.8
top quark	t	$2e/3$	172.6

According to SM theory, the quarks cannot behave as free particles and they combine to form composite particles called hadrons such as baryons and mesons. Baryons consist of three valence quarks and the mesons with a valence quark and an antiquark. The most common baryons are the proton and the neutron; the basic building blocks of atomic nuclei. Pion and kaon can be given as examples for the mesons. The protons consist of two up and one down quark (*uud*), neutrons consist of one up and two down quarks (*udd*). Given that the baryons are included in the fermion family, they should obey the Pauli Exclusion Principle. There are some baryon states with three identical quarks (*uuu*). But this situation looks contradictory to the Pauli Exclusion Principle. To solve this problem, an extra property named as color charge which is carried by quarks and antiquarks was suggested. This was the birth of Quantum Chromo Dynamics (QCD). Each of the quarks has one of the three color charges as red, blue and green. So, since three quarks in the baryons have different colors, then they obey the Pauli Exclusion Principle and the problem mentioned above was solved in this way.

According to the SM, everything in the universe is made of the three generations of the elementary fermions and force carriers (mediators). The lightest and most stable elementary fermions are the first generation and every day matter is made of the first generation; whereas the unstable matter is made of the second and third generations. Up and down quarks with electron and electron neutrino belong to the first generation, charm and strange quarks with muon and muon neutrino belong to the second generation, top and bottom quarks with tau and tau neutrino belong to the third generation. The details of these elementary particles are given in Figure 1.1.

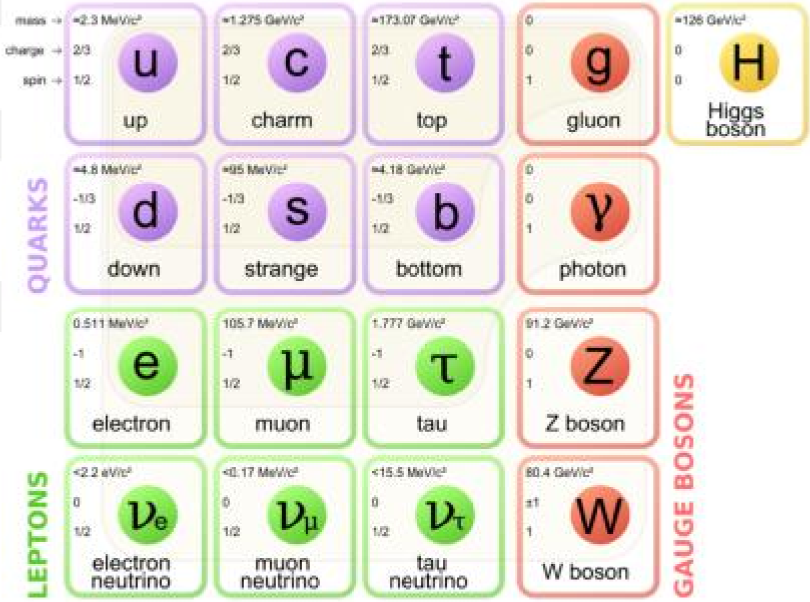

Figure 1.1. Fundamental particles of the SM (https://en.wikipedia.org/wiki/Standard_Model).

The interactions of the elementary particles are explained by the SM via four fundamental forces. Those forces are defined as: electromagnetic that is described by Quantum Electro Dynamics (QED), the strong that is described by the QCD, the weak force which is described by the weak theory. The electromagnetic and weak forces are unified as a single force which is called the electroweak force. The gravitational force is the fourth and the weakest of the all forces. All of these interactions take place with the exchange of gauge bosons.

The electromagnetic interaction occurs between particles having electrical charge and is responsible for connecting electrons to atoms or to molecules. Mediators of the electromagnetic interaction are photons. When distance between the particles increases, the effect of electromagnetic force decreases. Also, electromagnetic interaction has an infinite range.

The strong interaction holds protons and neutrons together in the nucleus, and also quarks in nucleons. It has a short-range and its mediators are gluons. The strong interaction which is the strongest of all the interactions has no effect above the distances greater than 10^{-15} m.

The weak interaction has very short-range and it plays an important role for the radioactive decays. The best typical example is beta-decay. The gauge bosons of the weak interaction are $W^{\pm}$ and Z^0. All weak interaction bosons have spin 1. Since the weak interaction bosons have very large mass they live very short so weak interaction has very short range.

The gravitational force is a force responsible for holding planets to stars, stars to galaxies and galaxies to galaxy clusters. The mediator particle of this force is a graviton which has not been discovered yet and it has spin 2. The range of the gravitational force is infinite. The effect of the gravitational force comes into prominence for the big masses, whereas its effect can be neglected in the particle physics.

The Higgs boson is defined as the source of mass of the matter and it has been discovered on 4 July 2012 at CERN. The mass of the Higgs boson was determined with a high statistics as m_H= 125.3±0.6 GeV (J. Beringer et al.). A schematic view of interactions between fundamental particles is shown in Figure 1.2.

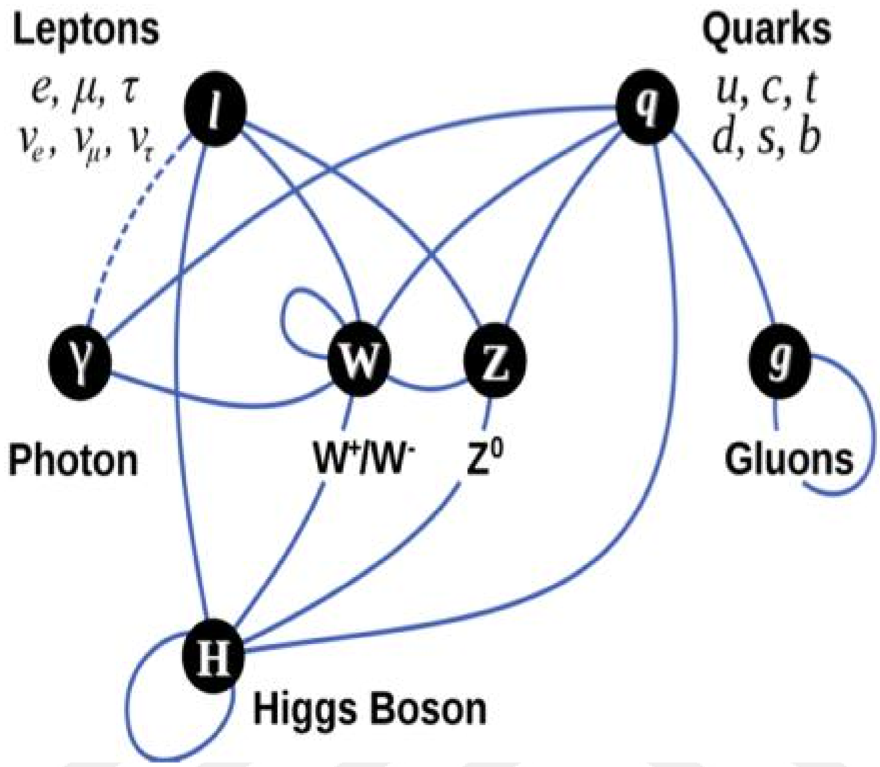

Figure 1.2. View of the interactions between the fundamental particles (http://en.wikipedia.org/wiki/Higgs_boson).

Despite the fact that the SM is the best theory and has passed from various experimental tests, there are some questions which are still unanswered by it. According to the SM, quarks and leptons are known as fundamental particles. One of the unanswered problems in the SM is: Are quarks and leptons fundamental particles or do they consist of other fundamental particles? There are other problems that wait an answer in the SM such as: If the observable universe is composed of the first generation quarks and leptons, why are there a second and third generation? Is there a fourth generation? Whenever any matter is created from energy in particle physics experiments, equal amounts of antimatter has to be created. Then, the universe should have created equal amounts of matter and antimatter. So why is there more matter then antimatter in the universe? This is also one of the questions that SM cannot explain. Another important question that cannot be solved by the SM is the unification of four fundamental interactions into one single force. The big mass difference between fundamental particles is one of the wondered issues by the high energy physicists. The answer of this question is clarified with the discovery of the Higgs particle which gives mass to all of the particles. One of the missing parts of the model has been completed with the discovery of the Higgs particle. So at this point, we can say that SM is not complete and the new physics beyond the SM is needed. There are some theories such as supersymmetry, string theory, Minimal Supersymmetric Standard Model (MSSM) to explain the deficiencies of the SM. To test these theories high energy experiments are needed. The four big experiments at CERN mentioned above are trying to test these theories.

This thesis includes performance analysis studies of hadronic barrel, hadronic endcap, hadronic outer and hadronic forward calorimeters which are sub calorimeters of the Hadronic Calorimeter (HCAL) of CMS experiment by using the 2015 cosmic and 13 TeV collision data. The main topic of this thesis is the HCAL performance analysis done by using the cosmic data that were taken in three different periods while the magnet was on or off. Also Beam Splash data which were taken in order to prepare the CMS detector were used in our analysis. This data that let us understand the behavior of HCAL are very important for the efficiency of the analysis. Furthermore, general performance of HCAL has been investigated in detail by contributing to 13 TeV collision data analysis and getting information about the status of each channel located in the calorimeter.

In the 2nd Chapter, general information will be given about the LHC and its experimental setup in detail. Section 2.2 gives information about the CMS and its sub-systems. Chapter 3 focuses on the analysis of HCAL performance and includes cosmic and collision data analysis. In chapter 4 the conclusion and results of this analysis will be given.

2. EXPERIMENTAL OVERVIEW

CERN has the most important and the biggest accelerator complex of the world. It is located on the border between Switzerland and France. Approximately over 10,000 scientists and engineers from over 100 countries and 600 institutes work at CERN. Physicists and engineers probe the fundamental structure of the universe at CERN. For this purpose, they use one of the biggest particle accelerators named as Large Hadron Collider (LHC) (http://home.cern/about).

LHC is a proton-proton (p-p) accelerator that is the biggest in size and the highest in energy in the world. There are many experiments located at the LHC. These experiments are called as A Toroidal LHC Apparatus (ATLAS), Compact Muon Solenoid (CMS), A Large Ion Collider (ALICE), Large Hadron Collider beauty (LHCb), Large Hadron Collider forward (LHCf) and TOTal Elastic and Diffractive Cross Section Measurement (TOTEM). This chapter is dedicated to explain all these experiments shortly except the CMS which is the experiments that is studied in this thesis.

2.1. Large Hadron Collider

The LHC is the highest-powered proton and ion accelerator in the world. It has been built 100 m underground. The length of the accelerator ring is 27 km. Before the LHC, the same tunnel was used for the Large Electron Positron (LEP) collider until 2000.

The proton-proton and heavy ions are collided in the LHC. The designed center of mass energy is $\sqrt{s}$ = 14 TeV ($\sqrt{s}$ = 5.5 TeV) and the luminosity is 10^{34} cm^{-2} s^{-1} (10^{27} cm^{-2} s^{-1}) for proton-proton (heavy ion) collision. The luminosity is directly proportional to collision number and is given by:

$$L = \frac{N_b^2 n_b f_{rev} \gamma F}{4\pi \epsilon_n \beta^*}. \qquad (3.1)$$

where N_b is the number of particles per bunch, n_b is the number of bunches per beam, f_{rev} is the revolution frequency, γ is the relativistic gamma factor, ε_n is the normalized transverse emittance, β^* is the beta function at the interaction point, F is the geometric luminosity reduction factor (Evans and P.B, 2008).

In LHC, the particle beams move in opposite directions through the circular ring. The most important part of the collider is the superconducting dipole magnets. They keep the protons in the orbit and must be kept approximately at $-271^{o}C$. Therefore, liquid helium is used in order to cool magnets and related materials. The superconducting magnets that consist of 154 dipoles and 54 quadrupoles are located in each part of the LHC. The dipole electromagnets keep particle beams in orbit in the vacuum pipe. The particle beams are focused by using quadrupole electromagnets (http://home.web.cern.ch/topics/large-hadron-collider).

Before being injected into the LHC, proton beams are accelerated by many different accelerator systems to reach the intended energy. At the first stage, protons are accelerated in the linear accelerator (LINAC2) to energy of 50 MeV and immediately the after energy of the beam is brought up to 1.4 GeV by the Proton Synchrotron Booster (PSB). Subsequently the protons are injected to the Proton Synchrotron (PS) which in turn accelerates them to energy of 26 GeV and then proton beams are accelerated up to 450 GeV in the Super Proton Synchrotron (SPS). At the end, proton beams are injected into LHC and accelerated up to energy of 7 TeV. Collisions take place at the four interaction points which are located in the LHC ring at every 25 nanoseconds.

The first proton beams were circulated at 10 September 2008 in the ring of the LHC. Because of the faulty connection between two superconducting magnets, operation was halted. After the technical repairs, the proton beams were successfully started to circulate again in 20 November 2009 at the center of mass energy of $\sqrt{s}$ = 4 TeV. In March 2010, two proton beams were collided at the center of mass energy of $\sqrt{s}$ = 7 TeV. In 5 April 2012, p-p collisions with a center of mass energy of $\sqrt{s}$ = 8 TeV were seen in the LHC. In 14 February 2013, the LHC was shut down for a technical stop for two years. During this technical stop, scientists and engineers worked to repair or replace the problematic accelerator and detector components.

After completing the renovation studies, two proton beams were collided at center of mass energy of $\sqrt{s}$ = 13 TeV in 21 May 2015. Thus, the physics program of the LHC began again and many physics runs were taken in this period.

The accelerated proton beams are collided at the center of the three big experiments. ATLAS and CMS are two general-purpose detectors. The other two big experiments are ALICE and LHCb. TOTEM and LHCf are the smaller experiments which take data for specific physics analysis. These experiments will be explained briefly in this chapter. The CMS, ATLAS, ALICE and LHCb are placed in the four underground caverns that are distributed around the main ring. The CMS and ATLAS are comprehensive experiments but with slightly different designs. Dark matter, supersymmetry (SUSY), SM and Higgs boson are few subjects searched at these experiments. To detect all particles coming from the collisions, both CMS and ATLAS experiments have been designed in structures which look like an onion as other high energy experiments do. ATLAS experiment uses a toroidal magnet, while CMS experiment uses a solenoid magnet. This is one of the main differences between two experiments. Also, CMS is the heaviest detector in terms of its mass, while ATLAS is the biggest detector in terms of its size. The ALICE experiment is smaller compared to CMS and ATLAS. It is designed to investigate the structure of quark-gluon plasma that occurred on the sidelines of the formation of universe, whereas the LHCb experiment is built to study asymmetry between matter and antimatter in the b-quark system. TOTEM and LHCf are small experiments which focus on forward particles. Figure 2.1 shows CERN accelerator complex and experiments in it (https://home.web.cern.ch/about/experiments).

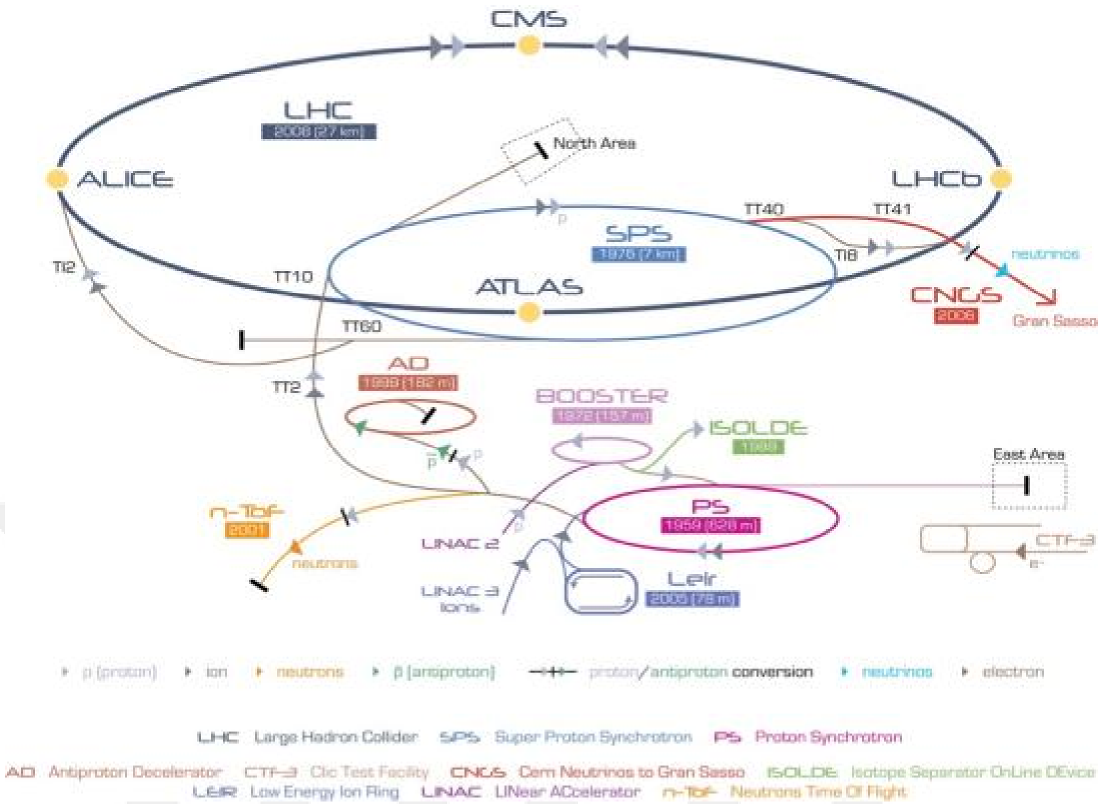

Figure 2.1. Overview of the CERN accelerator complex and LHC experiments (http://te-epc-lpc.web.cern.ch/te-epc-lpc/machines/pagesources/Cern-Accelerator-Complex.jpg).

2.1.1. A Large Ion Collider

A Large Ion Collider **(**ALICE) is customized as a heavy-ion detector which collides heavy nuclei (Pb-Pb and Au-Au) in its center in order to investigate physics of the strong-interacting matter called as quark-gluon plasma. The overall dimensions of the ALICE detector are a length of 26 m, a height of 16 m, and a width of 16 m. Also, total weight of it is about 10 000 t. It consists of 18 sub-detectors to identify tens of thousands particles that are produced at each of heavy ion collisions and to determine the tracks or particles. Schematic view of the ALICE experiment is given Figure 2.2 (CERN Brochure, 2010).

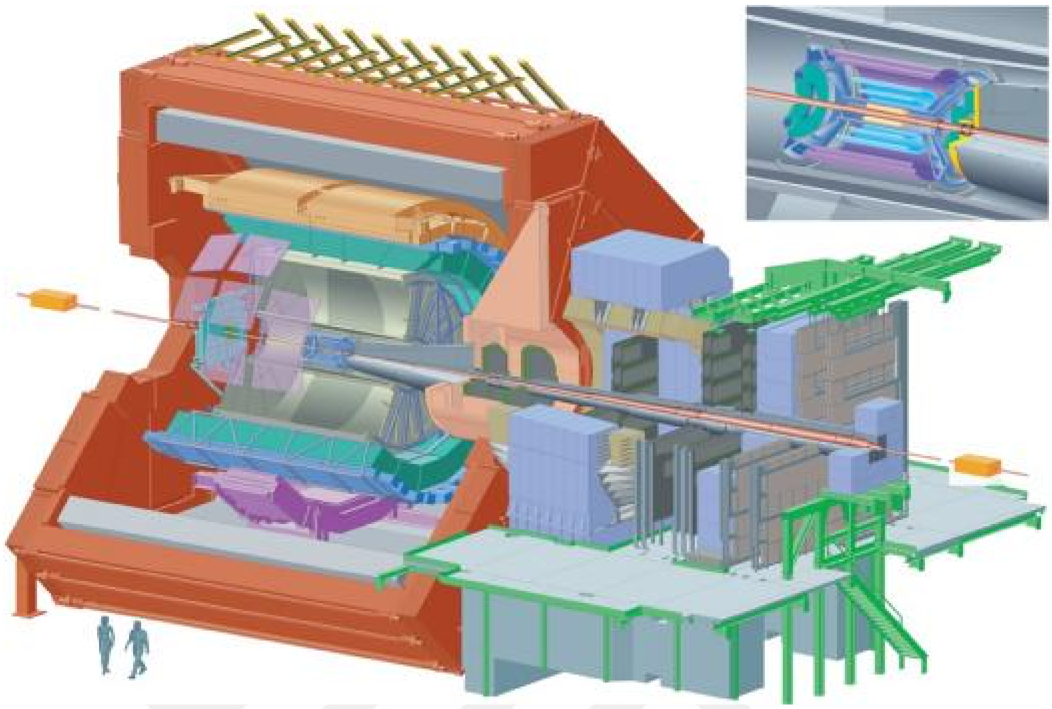

Figure 2.2. Schematic view of the ALICE experiment (http://aliceinfo.cern.ch./Public /Objects/Chapter2/ALICESetUp-NewSimple.jpg).

ALICE detector is designed to understand the time slot immediately after the big bang and provide information for the conditions during early universe. The quark-gluon plasma is assumed to exist immediately after the big bang. The ALICE experiment will set light to scientific world by understanding structure of the quark-gluon plasma using Pb-Pb collisions. The all ordinary matter consists of atoms in the apparent universe. Each atom contains a nucleus which is composed of protons and neutrons named as nucleons. Proton and neutron are made of quarks which are bounded each other strongly via gluons. This connection is very powerful and since quarks carry color quantum number they cannot exist in free form. This is known as color confinement. In the specific time ranges of every year, the LHC collides heavy ions and it tries to create same conditions that are immediately after the Big Bang in the laboratory conditions. At these collisions, the temperature is a hundred thousand times greater than the temperature in the center of the sun. In these extreme conditions, the nucleus starts to melt and quarks and gluons are released by protons and neutrons. This state of matter is known as the quark-gluon plasma. Understanding of the properties of quark-gluon plasma is the key issue in QCD and color confinement phenomenology. Over than 1500 scientists coming from 154 physics institutes in 37 countries study about the quark-gluon plasma structure (https://home.web.cern.ch/about/experiments/alice).

2.1.2. A Toroidal LHC Apparatus

A Toroidal LHC Apparatus (ATLAS) is one of the two general purpose experiments at the LHC. It investigates various physics issues such as Higgs boson, dark matter, extra dimensions and physics beyond SM. Even though it has the same scientific aims as the CMS experiment, ATLAS uses slightly different detector systems and a different magnet-system design. The ATLAS detector measures momenta, energies and orbits of particles through six different detecting sub-system arranged in layers around the interaction point. A huge superconducting toroidal magnet system bends the paths of charged particles coming from interaction point. Thus, their momenta can be measured sensitively. The ATLAS experiment played a role in discovery of the Higgs boson together with CMS experiment. Given that the interactions in the ATLAS detector create an enormous flow of data, it uses advanced trigger, data-acquisition and computing system to compile these data. The overall dimensions of the ATLAS detector are a length of 46 m, a height of 25 m, and a width of 25 m. A weight of the ATLAS that is the largest volume particle detector ever constructed is a 7000 t. About 5000 scientists from 180 institutes in 38 countries works for the ATLAS experiment. An overall picture of the ATLAS can be seen in Figure 2.3 (https://home.web.cern.ch/about/experiments/atlas).

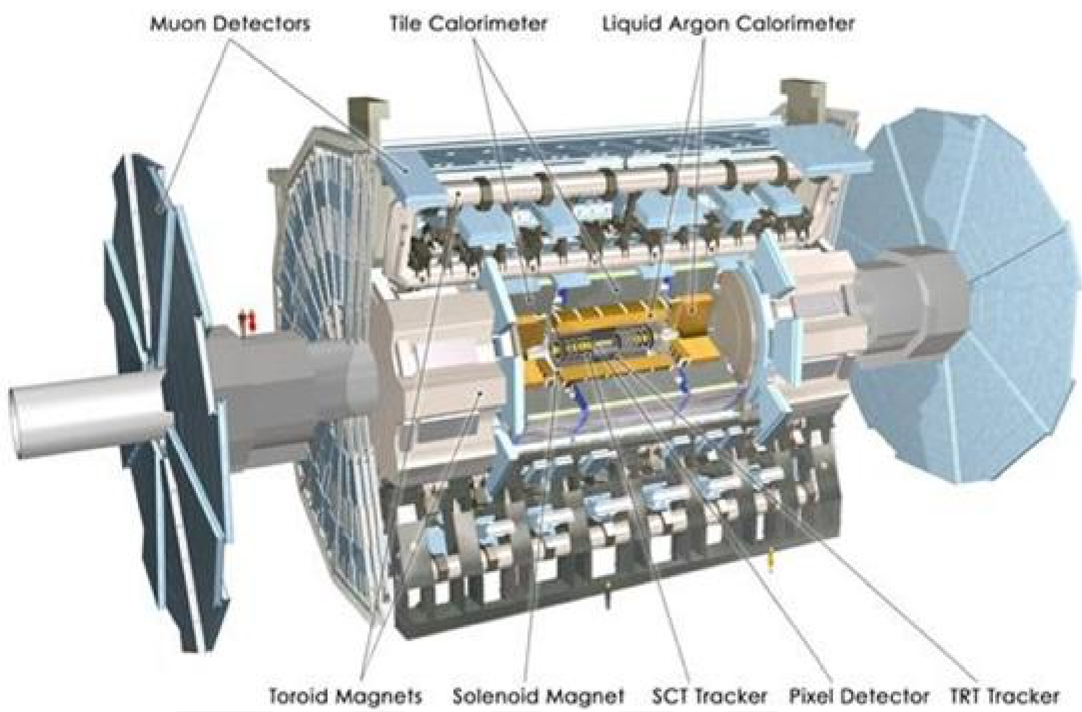

Figure 2.3. Schematic view of the ATLAS detector and its components.

2.1.3. Large Hadron Collider beauty

Large Hadron Collider beauty (LHCb) experiment is one of the four big experiments at the LHC ring. Main goal of the LHCb is to investigate a slight asymmetry between matter and anti-matter in interactions of particles with bottom quarks. The overall dimensions of the LHCb detector are a length of 21 m, a height of 10 m and a width of 13 m. Also, it has total weight of 5600 t. The structure of LHCb detector does not look like an onion. It looks like slice of onion. It also uses a series of sub-detectors in order to detect mainly forward particles but it does not cover the entire interaction point. The first sub-detector is mounted close to the interaction point; other detectors are mounted one after another over a length of 20 m. About 731 scientists from 66 different universities work on the LHCb experiment. Schematic view of the LHCb experiment is shown in Figure 2.4 (https://home.web.cern.ch/about/experiments/lhcb).

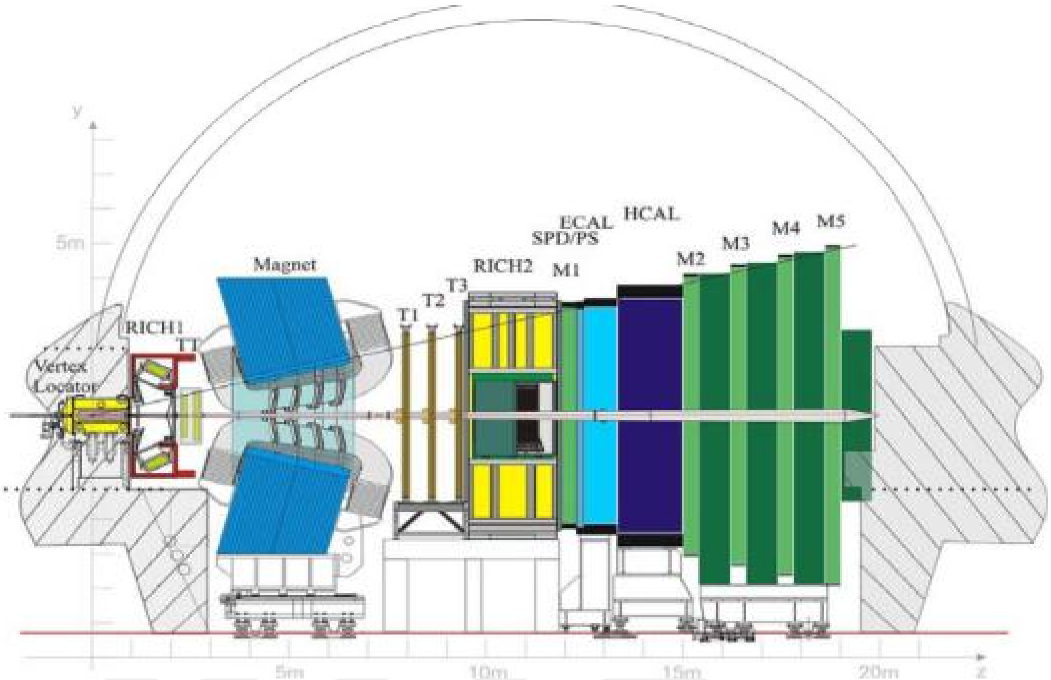

Figure 2.4. Schematic view of the LHCb experiment.

2.1.4. Large Hadron Collider forward

The Earth is continuously exposed to the bombardment of the cosmic rays coming from the space. When cosmic rays arrive to the atmosphere of the Earth, they interact with the atmosphere and then produce particle showers. The Large Hadron Collider forward **(**LHCf) experiment uses particles which are thrown at forward directions by the LHC interactions in order to simulate the cosmic rays in laboratory conditions. LHCf is made up two detectors which are self-contained and sit along the LHC beam line, at 140 m either side of the ATLAS collision point. Each of the two detectors of the LHCf experiment has a length of 30 cm, a high of 10 cm, a width of 10 cm and a weight of 40 kg. 30 scientists from 12 institutes in 6 countries work on the LHCf experiment. A schematic view of the LHCf detector is given in Figure 2.5 (https://home.web.cern.ch/about/experiments/lhcf).

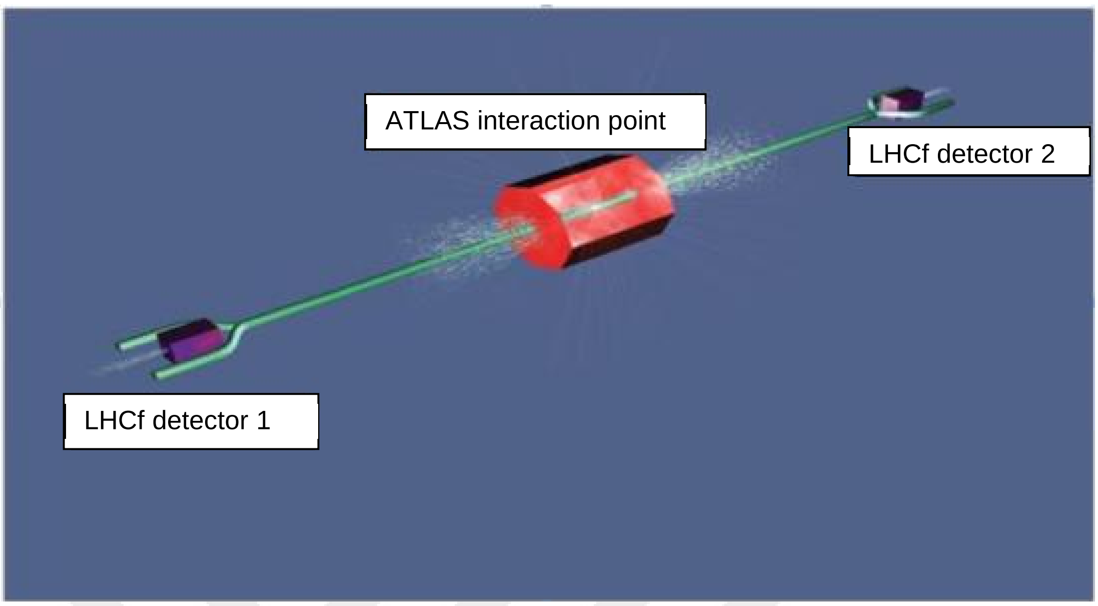

Figure 2.5. Overview of the LHCf experiment (CERN Brochure, 2009).

2.1.5. TOTal Elastic and Diffractive Cross Section Measurement

The TOTal Elastic and Diffractive Cross Section Measurement (TOTEM) experiment is designed to record secondary particles coming from LHC collisions and have the same directions with proton beams, sensitively. Also, proton-proton cross section is measured by the TOTEM experiment in order to understand the structure of protons in detail. TOTEM detectors are located at almost half a kilometer around either side of the CMS interaction point. TOTEM experiment has 26 Roman pots detectors which are positioned at beam line at either side of the CMS detector. The overall dimensions of the TOTEM detector are a height of 5 m, a width of 5 m and a length of 440 m. Also, it has a weight of 20 t. About 21 different institutes work for the TOTEM experiment. The TOTEM experiment and TOTEM Roman pots detectors are shown in Figure 2.6 (http://totem-experiment.web.cern.ch/totem-experiment/detectors).

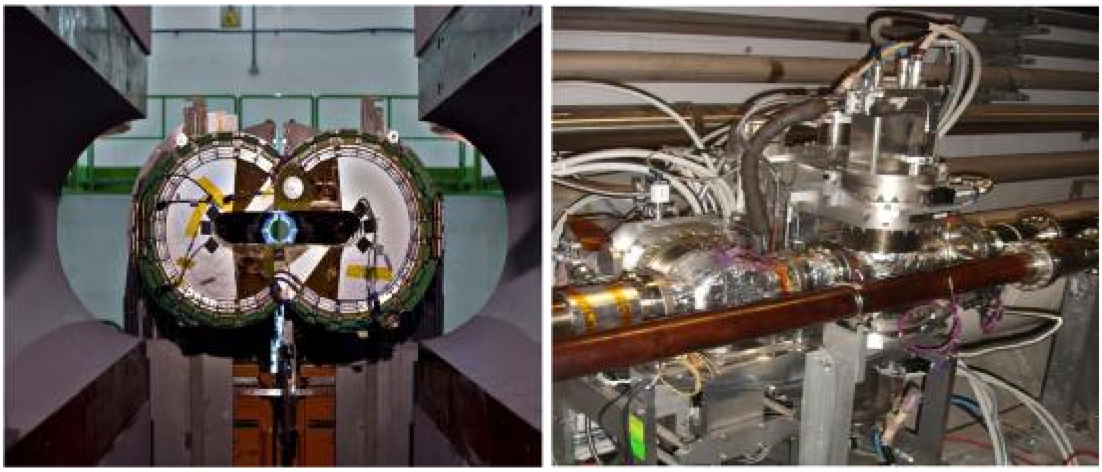
Figure 2.6. TOTEM experiment and TOTEM Roman pots.

2.2. Compact Muon Solenoid

The Compact Muon Solenoid **(**CMS) experiment is one of the two general purpose detectors which are designed to run at the highest luminosity and center of mass of energy of $\sqrt{s}$ = 14 TeV. It was located inside one pit of the LHC 100 m under ground near by the Cessy, French side. CMS detects particles which have different features. It measures energies and momenta of these particles sensitively thanks to the cylindrical shape that consists of many layers of different detectors. The goal of the CMS is to search for new physics beyond the SM such as black holes, super symmetry, dark matter, origin of mass and so on. To discover new physics, CMS uses various detector systems which have different features. The general requirements for the CMS detector are following:

- Good muon identification and momenta resolution in wide range of angles, good dimuon mass resolution (1% at 100 GeV) at high accuracy, ability to determine charge of muons,
- Good momenta resolution for charged particles and reconstruction efficiency in the inner tracker system. Influential triggering and tagging for τ and b jets,
- Good electromagnetic energy resolution in high efficiency, good mass resolution of diphoton and dielectron (1% at 100 GeV) and π^0 rejection,

- Good missing transverse energy and dimass resolution, requiring hadron calorimeter has large hermetic geometric coverage.

The main part of the CMS is a large superconducting solenoid magnet that provides a 3.8 T field. The superconducting magnet measures momenta of charged-particles. Starting from the point closest to the interaction region, the individual subdetectors which encircled by a superconducting solenoid are the silicon based Inner Tracking System, the homogeneous Electromagnetic Calorimeter (ECAL) and the hermetic Hadronic Calorimeter (HCAL), the outer system consist of layers of muon detectors and hadronic outer (HO) calorimeter. The transverse section of CMS detector is given in Figure 2.7.

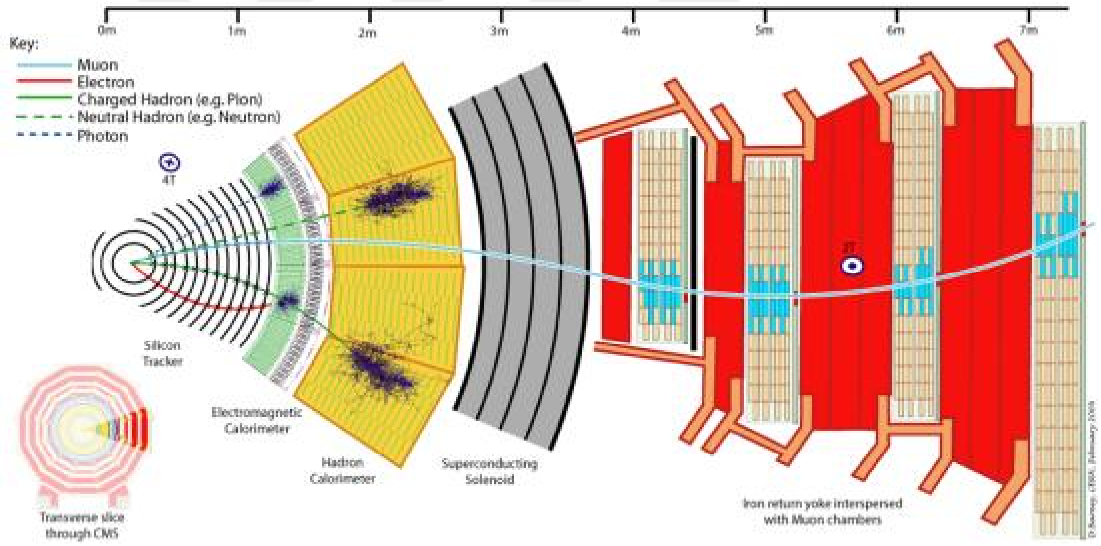

Figure 2.7. Transverse section of the CMS detector.

The overall dimensions of the CMS detector are a length of 28.7 m, a height of 15 m, a width of 15 m and a total weight of 14000 t. Over than 3300 scientists from 42 countries, 189 institutes work for the CMS experiment. Schematic layout of the CMS is shown in Figure 2.8.

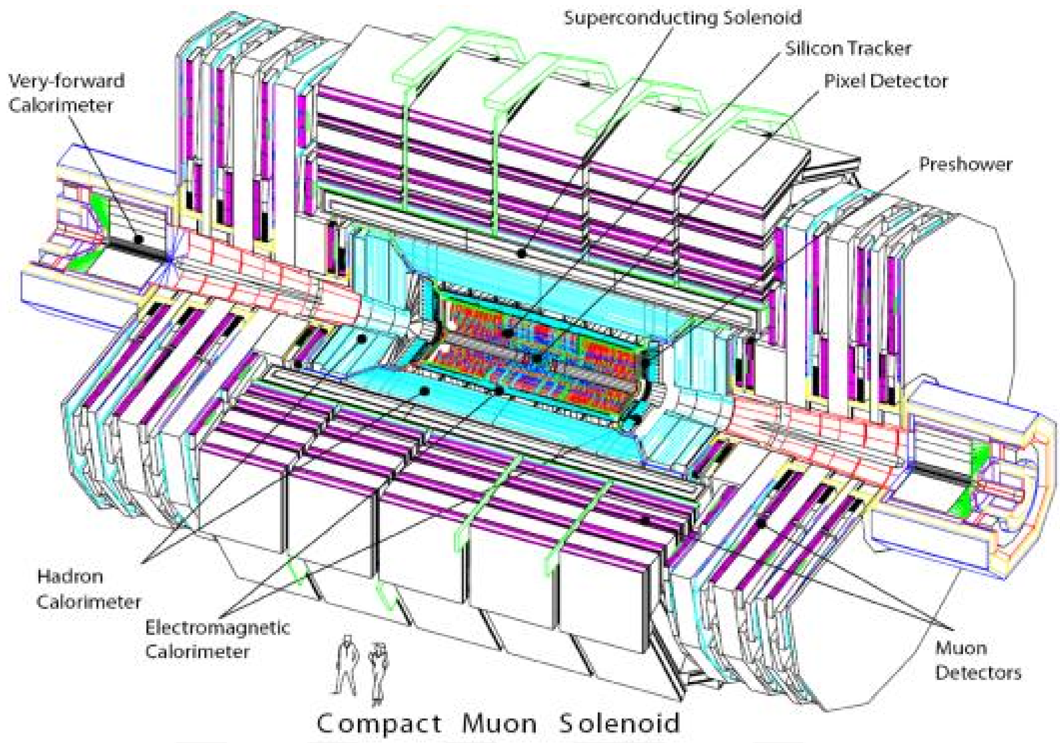

Figure 2.8. Schematic layout of CMS (CMS TDR, 2006).

The CMS Coordinate Frame: The CMS uses a right handed cylindrical coordinate system (θ, φ, z) whose origin is the interaction point of p-p at CMS. The z-axis along the beam direction, the y-axis points vertically upward and the x-axis points horizontally towards the center of the LHC. z, y and x-axis are orthogonal to each other. The azimuthal angle φ is measured from the x-axis in the x-y plane and the radial coordinate is symbolized by r in this plane. The polar angle θ is measured from the z-axis. Pseudorapidity is described as $\eta = -\ln \tan(\theta/2)$, also the rapidity is identified as $y=\frac{1}{2} ln \frac{E+p_z}{E-p_z}$. The transverse momentum P_T and transverse energy E_T of the particles are calculated from the x and y components respectively. The CMS coordinate system is given in Figure 2.9 (CMS TDR, 2006).

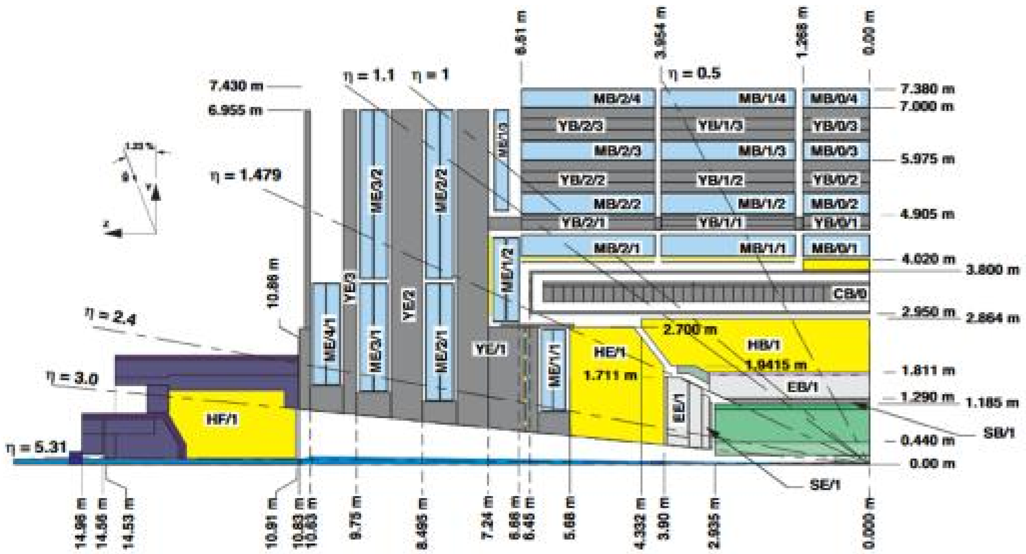

Figure 2.9. Longitudinal view of one quarter of the CMS detector and its coordinate system (https://inspirehep.net/record/837874/files/CMSview1.png).

2.2.1. The Inner Tracking System

The inner tracker system is a detector which is the closest one to the beam interaction point. The CMS tracker is made entirely of silicon. The momentum of particles plays an important role for the particle identification. The goal of the tracker system is to determine momentum and secondary vertices of charged particles and to provide the measurement of the particle trajectories sensitively. When the charged particles enter the magnetic field, their paths are bent by the Lorentz force. Particles which have high momentum are less bent compared to low momentum particles. One of the methods used to find momentum of a particle is to measure their bended trajectories in the detector. CMS tracker system can reconstruct the path of high energy particles by using this method. The inner tracker system is a cylinder that encloses the interaction point. It covers the pseudorapidity region of $|\eta| < 2.6$ and has 5.8 m length, 1.2 m radius. The tracker system of CMS consists of three layers of silicon pixel detector and ten layers of silicon strip detector. Each system is completed by endcaps which are consists of two pixel disks and twelve strip disks. They are placed on the each side of the barrel. Given that the tracker detector is a detector which is closest the interaction region, it exposes to intense radiation.

Therefore, it was designed using materials which are resistant to radiation. The schematic view of the CMS inner tracking system is given in Figure 2.10.

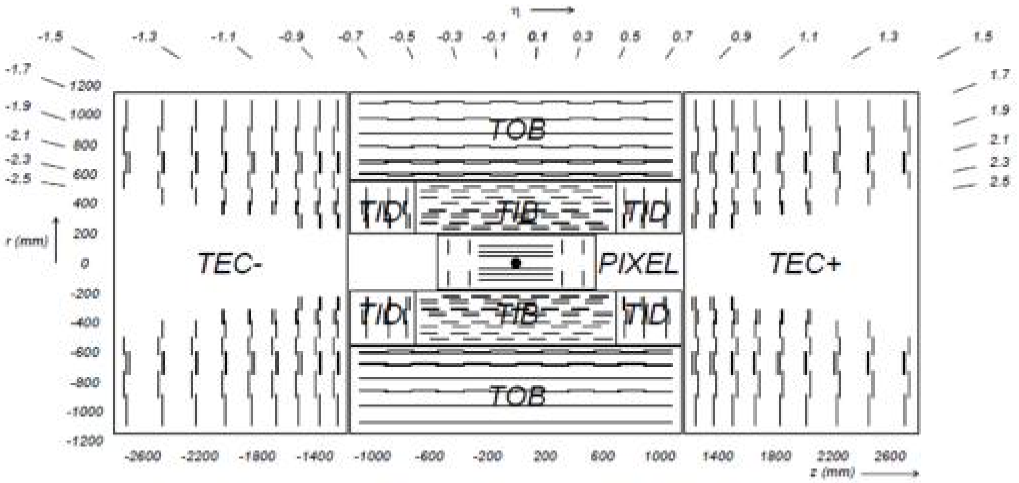

Figure 2.10. Schematic cross section through the CMS tracker. Each line represents a detector module (CMS Collaboration, 2008, JINST 3 S08004).

2.2.1.1. The Pixel Detector

The pixel detector called as the vertex detector consists of 66 million silicon pixel sensors which have a surface of 100 μm × 150 μm and thickness of 300 μm. The pixel tracker located in the central region which is close to the interaction point is designed to provide 3-dimensional vertex structuring and identification of τ and b jets. Pixel detector consists of three pixel barrels and two endcaps. It covers the pseudorapidity region of $|\eta| < 2.5$. Length of the barrel layers is 53 cm and positioned at mean radii of 4.4 cm, 7.3 cm and 10.2 cm respectively. Two endcap layers are regulated in like a turbine shape with 20^o tilt, extending from 6 to 15 cm in radius and are placed at 34.5 cm and 46.5 cm from the interaction point. The pixel detector system consists of a total of 1440 detector module and 16000 readout modules. Geometrical layout of the pixel detector system is shown in Figure 2.11 (CMS Collaboration, 2008, JINST 3 S08004).

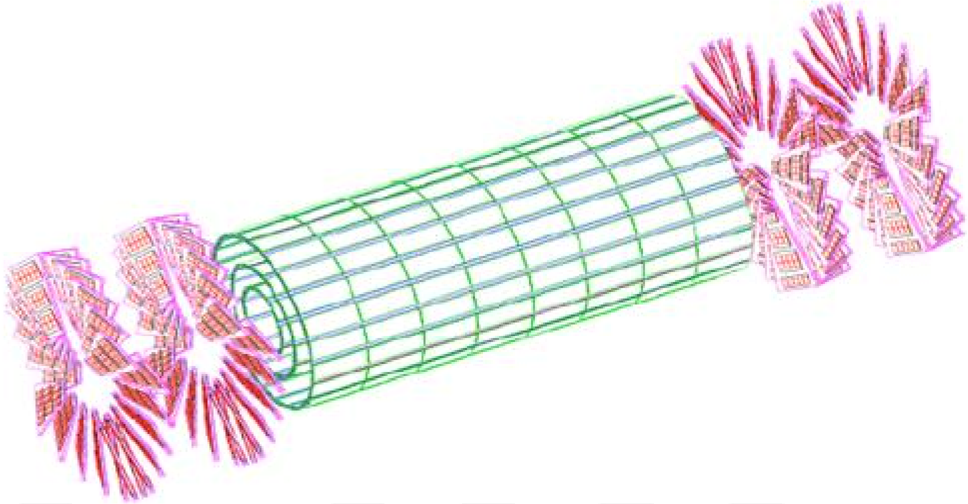

Figure 2.11. An illustration of the Pixel detector (CMS TDR, 2006).

2.2.1.2. The Silicon Strip Detector

The silicon strip detector enclosing the pixel detector is the biggest silicon detector ever constructed. It consists of two concentric Tracker Inner Barrel (TIB), Tracker Outer Barrel (TOB), Tracker Inner Disk (TID) and Tracker End Caps (TEC). The total an active area of the silicon strip detector is close to 207 m^2. TID consists six disks which is three on each side of the collision point located at distance of z = ±7.67 cm, ±62 cm and ±103.57 cm respectively. TEC layers are located at distance of z = ±46 cm. A geometrical layout of the silicon strip tracker is given by Figure 2.12.

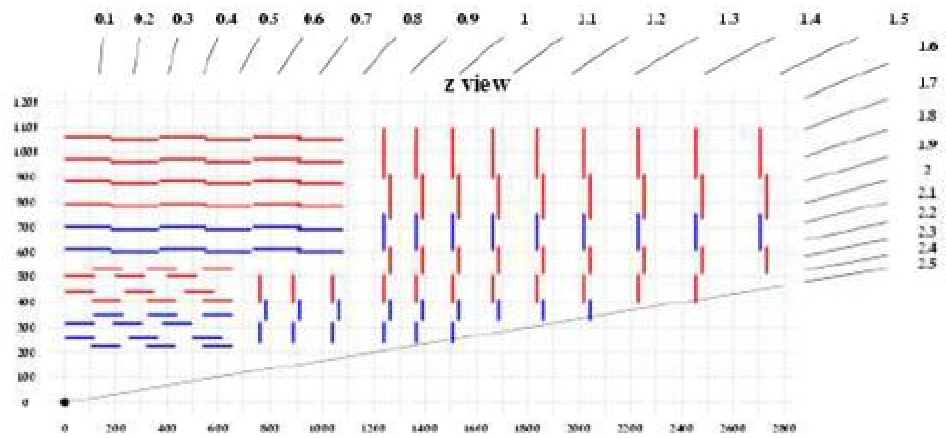

Figure 2.12. A sketch of the longitudinal view of a quarter of the silicon strip detector. Mono modules are represented by red, stereo modules by blue.

2.2.2. The Calorimeter System

The CMS calorimeters are designed to stop primary particles such as electrons, protons and hadrons that emerge from collisions and measure their energies with a high resolution. The main components of the CMS calorimeter system are electromagnetic calorimeter (ECAL) and hadronic calorimeter (HCAL). The CASTOR (Centauro And Strange Object Research) and ZDC (Zero Degree Calorimeter) are located in the CMS forward region. ECAL is used to measure of electrons and photons via electromagnetic interactions, whereas HCAL is used to measure energies of charged and uncharged hadrons via strong interactions.

2.2.2.1. Electromagnetic Calorimeter

The electromagnetic calorimeter is designed to measure energies of particles which interact electromagnetically such as electron and photon with very high precision. Also, it is designed to detect electrons and photons coming from Higgs decay processes H → γγ (m_H < 150 GeV), H → ZZ and H → WW for 125 GeV < m_H < 700 GeV. The channel in which Higgs decayed into two photons (H → γγ) is an important channel to determine photons with high precision and is used to optimize energy resolution of ECAL.

The ECAL is a hermetic homogeneous calorimeter made of 76000 lead tungstate ($PbWO_4$) crystals which is extremely dense and is placed inside the magnetic coil, outside of the tracker. Dimension of each crystal is 22 mm × 22 mm × 230 mm. Because of its radiation resistance, the lead tungstate crystals which have a very high density (8.28 g / cm^3), short radiation length (X_0= 0.89 cm) and small Moliere Radius (***r*** = 2.2 cm) were chosen for the ECAL. The crystals are transparent completely although 98% of masses of these crystals are metal. Also crystals are very fast (about 80% of the scintillation light is emitted within 25 ns). The ECAL composes of three main components: Electromagnetic Barrel (EB), Electromagnetic Endcap (EE) and Electromagnetic Preshower (ES). Figure 2.13 shows three main components of the ECAL (CMS Collaboration, 2008, JINST 3 S08004).

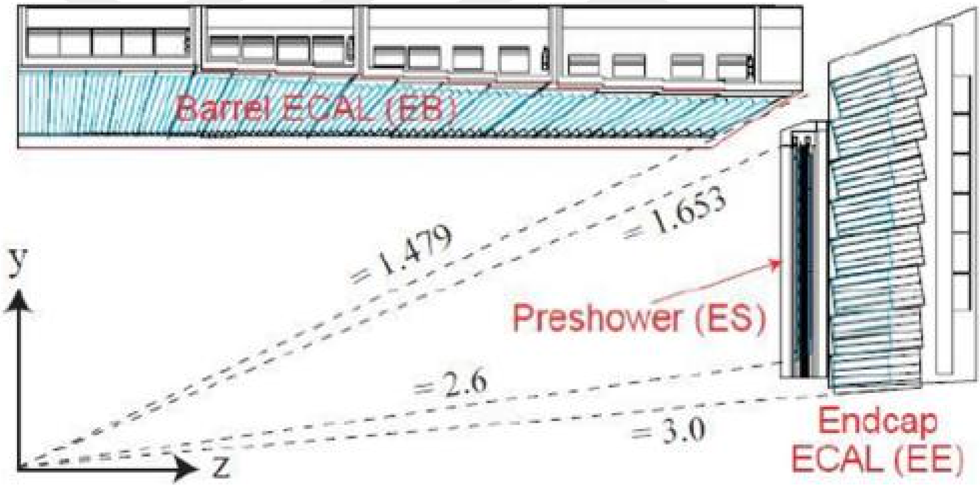

Figure 2.13. A quarter view of the CMS electromagnetic calorimeter layout.

Electromagnetic Barrel Calorimeter: The electromagnetic barrel (EB) of CMS covers the pseudorapidity range of $|\eta| < 1.49$. The cylindrical barrel has an inner radius of 129 cm and consists of 36 super modules which contain 1700 crystals. The crystals have a trapezoidal shape. The crystal cross section is 22 × 22 mm^2 at the front face of the crystal and 26 × 26 mm^2 at the rear face and their length is 23 cm corresponding to $25.8X_0$. Here X_0 is a radiation length of the crystal material. Total volume of the barrel section is 8.14 m^3, a weight of 67.4 t and the granularity of the barrel is $\Delta\eta \times \Delta\varphi = 0.0175 \times 0.0175$. In the barrel section, the scintillation light is handled by silicon avalanche photodiodes (APDs). Each APD has 5 × 5 mm^2 active area and they are mounted in pairs to each of the crystal. The signal gain of APD is around 50 at the 18^oC.

Electromagnetic Endcap Calorimeter: The electromagnetic endcap (EE) covers the pseudorapidity range of 1.479 < $|\eta|$ < 3.0 and is located 3.17 m away from the interaction point. The endcap section consists of 5 × 5 crystals which is called as SuperCrystals (SCs) and these are assembled into two endcap halves called Dees. The endcap composes of 7324 crystals which have dimension of 28.6 × 28.6 × 220 mm^3. A length of crystals is 22 cm corresponding to $24.7X_0$. The scintillation light is handled by vacuum photo triodes (VPTs) which is resistant to radiation in the endcap section. VPTs are photo multipliers which have a single gain stage and these devices are specially designed for CMS. Each VPT has radius of 25 mm and a cross section of about 280 mm^2. One VPT is located at the rear of the each crystal.

Electromagnetic Preshower Detector: The electromagnetic preshower detector (ES) is located in front of the endcap modules and covers most of the endcap surface. It is made of lead and silicon strips and has a thickness of $3X_0$. The main goal of its design is to determine neutral pions (π^0) in the endcaps within the eta region of 1.653 < $|\eta|$ < 2.6. ES is also used for the identification of electrons from minimum ionizing particles, and provides better measurement of the position of electrons and photons with high granularity (CMS TDR, 2006).

2.2.2.2. Hadron Calorimeter

The CMS calorimeter system is completed with the hadronic calorimeter (HCAL). The HCAL is located just outside of the electromagnetic calorimeter, inside the superconducting magnetic coil. It covers the pseudorapidity region of $|\eta|$ < 5.0. HCAL is designed to measure energies of both charged and uncharged hadrons such as proton, neutron, kaon and pion generated in p-p collisions. It plays an important role to determine energies of hadronic showers and jets as well as their directions and also determines missing transverse energy with a high precision. The general requirements for the HCAL:

- High hermeticity,
- Moderate energy resolution,
- Good transverse granularity,
- Sufficient depth for hadron showers.

Sampling calorimeter system is designed to provide these requirements. The HCAL is a sampling calorimeter that consists of brass and stainless steel absorber and 70000 active plastic scintillator tiles.

HCAL consists of four main parts: hadronic barrel (HB), hadronic endcap (HE), hadronic outer (HO) and hadronic forward (HF). HB and HE calorimeters are located inside of the solenoid magnet and just outside of the ECAL. They cover the pseudorapidity range of $|\eta| < 3.0$. Given that the HB is located between ECAL and solenoid magnet, it cannot completely absorb all hadronic showers. Therefore, HO is just located outside of the solenoid magnet and it provides absorption of hadronic showers coming from the barrel part. HF is located 11.2 m from the interaction point and covers pseudorapidity range of $3.0 < |\eta| < 5.0$. It is designed to determine energetic jets and measure missing transverse energy in the forward region.

Many signals come from different regions of the calorimeter. A projective geometry is generated in order to determine those signals. The calorimeter is divided into layers and towers. Thus, a mapping system is created. Because of the size of HCAL, it is divided into different depths to protect the whole calorimeter system from any malfunction that may occur. Thus, only part which is faulty is affected. Subsystems of the HCAL are shown in Figure 2.14.

Figure 2.14. Longitudinal view of HCAL indicating the locations of the HB, HE, HO and HF calorimeters (CMS Collaboration, 2008, JINST 3 S08004).

Hadronic Barrel Calorimeter: HB is a sampling calorimeter covering the pseudorapidity range of $|\eta| < 1.3$ and located between ECAL and superconducting solenoid magnet. HB consists of two half barrels, HB+ and HB−. Each half consists of 18 identical wedges that cover 20^o in φ and each wedge which has a weight of 26 t is segmented into four azimuthal angle ($\Delta\varphi = 5^o$) sectors. Each sector is segmented to 16 eta (η) called as a tower. The distance between the wedges is less than 2 mm and they are bolted together. The wedges consist of brass absorber plates which are known as C26000 cartridge brass that are parallel to the beam axis. These cartridge brass layers are composed of 70% Cu and 30% Zn elements. It has a density of ρ = 8.53 g / cm^3, a radiation length of X_0 = 1.49 cm and interaction length of λ_1 = 16.42 cm. The outermost and innermost layers are made up stainless steel for structural stiffness. The first layer of the absorber consists of 40 mm thick steel plate, followed by eight 50.5 mm thick brass plate, six 56.5 mm thick brass plates and 75 mm thick steel back plate. As an active material 17 active plastic scintillator tiles and wavelength shifting fibers (WLS) are inserted between the stainless steel and absorber brass layers. Each scintillator is arranged at a dimension of $\Delta\eta \times \Delta\varphi = 0.087 \times 0.087$ and is connected with a WLS fiber. The scintillation light is collected by 0.94 m diameter green double-cladded WLS fibers. The WLS fibers are spliced to clear optical fibers in order to reduce optical attenuation. The clear fiber goes to an optical connector at the end of the tray. An optical cable takes the light to an optical unit. The optical unit arranges the fibers into read-out towers and it provides transmission of light to hybrid photodiodes (HPD). Hybrid photodiodes are devices that convert light into electric current. Isometric view of HB wedges (left) and numbering scheme of wedges (right) are shown in Figure 2.15.

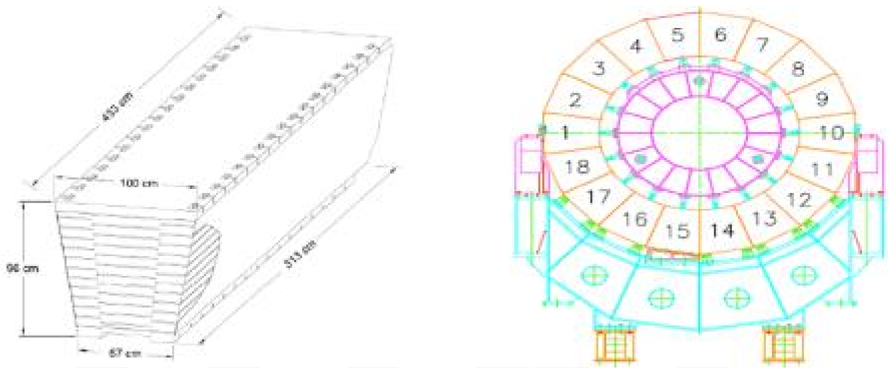

Figure 2.15. Isometric view for HB wedges (left), numbering scheme for HB wedges (right) (CMS Collaboration, 2008, JINST 3 S08004).

Each HB wedge contains 16 η towers. The η towers that are between 1 to 14 have a single depth, 15 to 16 have two depths. HB overlaps with HE calorimeter at the tower 16. HCAL tower segmentation is given by Figure 2.16.

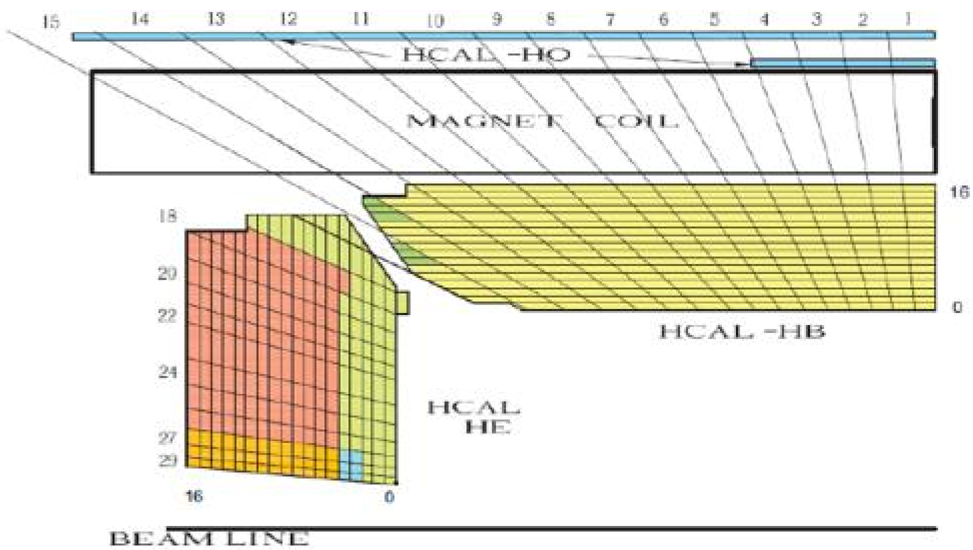

Figure 2.16. HCAL tower segmentation for HB and HE.

Hadronic Endcap Calorimeter: HE is a sampling calorimeter covering the pseudorapidity range of $1.3 < |\eta| < 3.0$ and located at the two ends of superconducting solenoid magnet. HE consists of two modules called as HE+ and HE−. Each module composes of 18 identical wedges that cover 20^o in φ and each wedge is segmented into four azimuthal angle ($\Delta\varphi = 5^o$) sectors. The granularity of the HE is identical with HB in $\Delta\eta \times \Delta\varphi = 0.087 \times 0.087$ for $|\eta| < 1.74$ and size of the segment doubles in region higher than $|\eta| > 1.74$. Given that the HE is placed at the end part of the magnet, the absorber part of the HE is made from a non-magnetic material. For this reason, C26000 cartridge brass that has good mechanical features and reasonable cost is used in the HE. The absorber has λ_1 = 16.4 cm interaction length, ρ = 8.83 g / cm^3 density and X_0 = 1.5 cm radiation length. The brass plates that are 79 mm thick are inserted to scintillator tiles with 9 mm gaps. The structure of absorber plates of HE is given in the Figure 2.17.

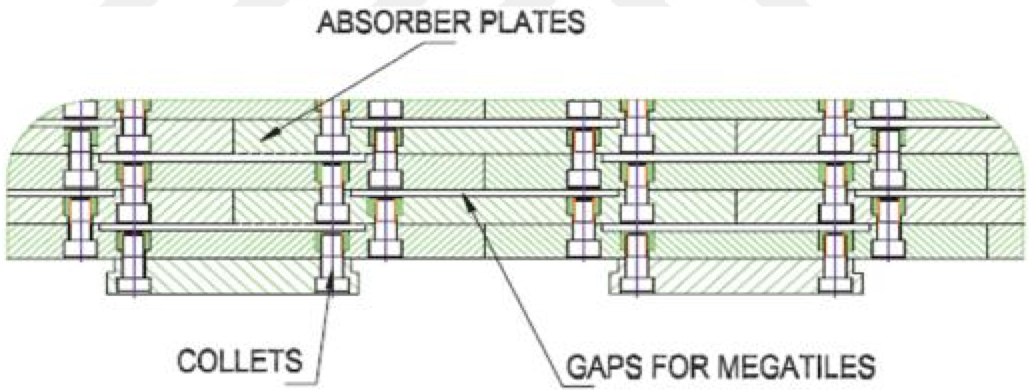

Figure 2.17. Mechanical structure of the HE absorbers.

The scintillation light is collected by WLS fibers in the HE and light is submitted to photo detectors via WLS fibers in suitable wavelength. The one end of fibers is covered with aluminum to increase the light collection. The other end of the fibers is spliced to a fiber optic cable which is connected to a photo detector. Signals are transferred to photo detectors by the optic cables. Multichannel HPD which has low accuracy against the magnetic field was used as a photo detector in the HE.

The HE calorimeter has 18 layers and consists of 14 tower and three different depths. Towers which are nearest the beam line (27 and 28) have 3 depths. The other towers have two longitudinal depths except tower 16 which overlap with the HB. The schematic view of HE and η segmentation in HE is given by Figure 2.18.

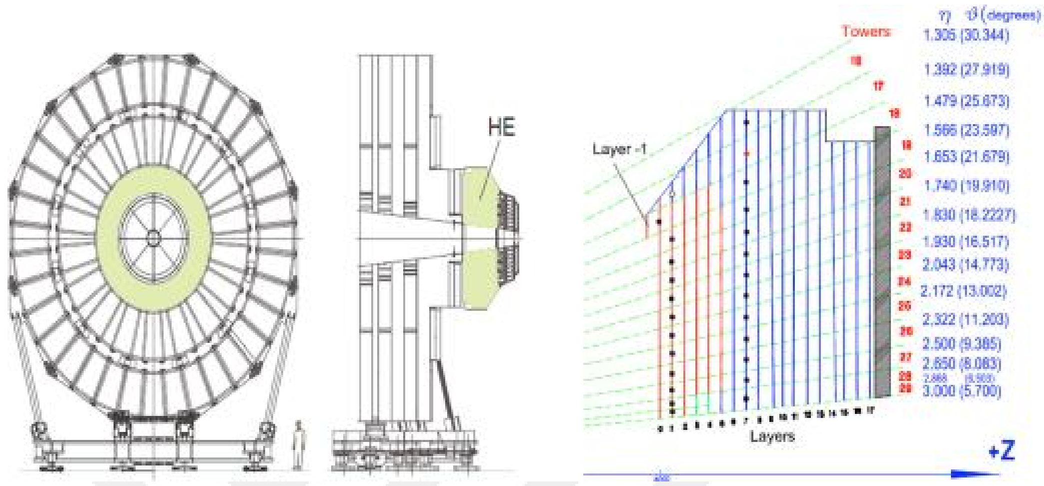

Figure 2.18. HE calorimeter (left), η segmentation in HE (right).

Hadronic Outer Calorimeter: In the central pseudorapidity region, since EB and HB have not sufficient thickness to ensure enough containment of the hadron showers, another hadron calorimeter is placed on the outer side of the magnet. HO is located just behind of the CMS magnet to ensure enough sampling, stop hadronic showers and measure missing transverse energy in high precision in pseudorapidity region of $|\eta| < 1.3$. The HO uses an additional absorber equal to $1/4 \sin\theta$ interaction length and used to identify showers which started late. The HO which is located just in front of the muon detector consists of five rings as muon detector or solenoid magnet and is placed as the first sensitive layer in each of the five rings. The rings are defined by the numbers −2, −1, 0, +1 and +2 with increasing η. This numbering is the same with the muon detector and increases through z- axis. A location of five rings in the z- axis is at −5.342 m, −2.686 m, 0, +2.686 m and +5.342 m respectively. Given that the HB has a minimum absorber depth in the $\eta = 0$, the ring 0 (central ring) has two HO layers. All other rings (±1 and ±2) have a single HO layer. As an absorber material iron plates are used which have a thickness of 19.5 cm in the central ring. The iron plates are placed at radial distances of 3.82 m and 4.07 m respectively. The position of HO layers is shown in Figure 2.19.

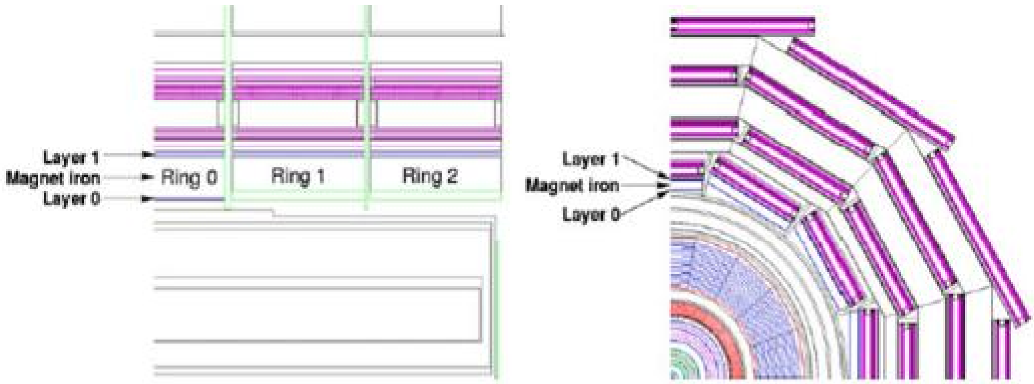

Figure 2.19. Longitudinal and transverse view of HO layers.

The geometrical structure of the HO calorimeter is designed properly to the geometry of the muon system. The HO is divided into sectors in the x−y plane as the HB calorimeter. Each ring of the HO calorimeter is divided into 12 identical sectors and these sectors are separated by 75 mm thick stainless steel beam. A sector in the HO calorimeter corresponds to $\Delta\varphi = 30^o$ and each sector is divided into 6 slices ($\Delta\varphi = 5^o$) in itself. The HO calorimeter composes of scintillator tiles which are one or two layers located in front of the first layer of the muon barrel detector. The scintillation light coming from tiles is collected by Y11 Kuraray WLS fibers which have diameter of 0.94 mm and transported to photo detectors. The scintillator tiles are packed into a single unit called as tray in order to install HO more easily. The schematic view of a HO tray is shown in Figure 2.20.

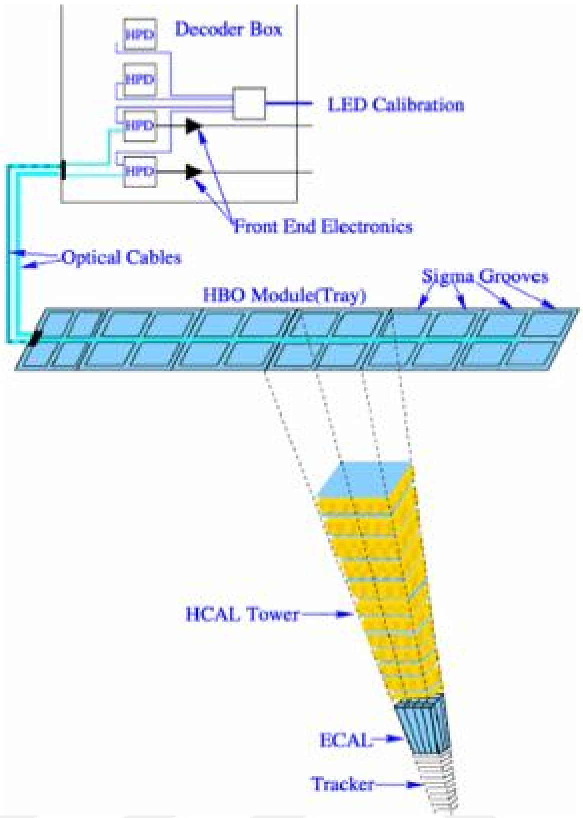

Figure 2.20. Schematic view of a HO tray shown with individual tiles (CMS Collaboration, 2008, JINST 3 S08004).

Hadronic Forward Calorimeter: The HF calorimeter covering the pseudorapidity range of $3 \leq |\eta| \leq 5$ is designed to determine hadronic jets in the forward region and measure missing transverse energy efficiently. The HF is located 11.2 m from the interaction point and consists of two modules that are placed on either side of the interaction point symmetrically called as HF+ and HF−. When the center of the beam line is taken as reference, the outer radius of HF calorimeter is 130 cm, the inner radius is 12.5 cm. The HF calorimeter consists of 36 identical wedges that cover 20^o in φ and each wedge has 26 η towers. Each of HF wedges has two sectors segmented with identical angle ($\Delta\varphi$ = 10^o). Given that the HF calorimeter is placed in the very forward region of the CMS, it is exposed to a very high radiation. When compared to other components of the CMS, the deposited energy in the each HF module is too much in each p-p collision. Therefore, steel absorbers and radiation hard quartz fibers inserted in these absorbers, were used as the active material in the HF. The quartz fibers which were placed in steel absorbers were aligned parallel to the beam axis. Two types of quartz fibers which have different lengths called as long and short were used in the HF calorimeter. The long fiber is referred as *L* and the short fiber as *S*. The length of the long fiber is 1.65 m. This fiber composes the electromagnetic part of HF and it is sensitive to particles interacted both electromagnetic and hadronic. The length of short fibers is 1.43 m and this fiber composes hadronic part of the HF. Hadronic part separates particles which interact electromagnetically from hadrons and provides energy measurement of hadrons. The schematic view of long and short fibers is given in Figure 2.21. The wedges of HF are shown is Figure 2.22.

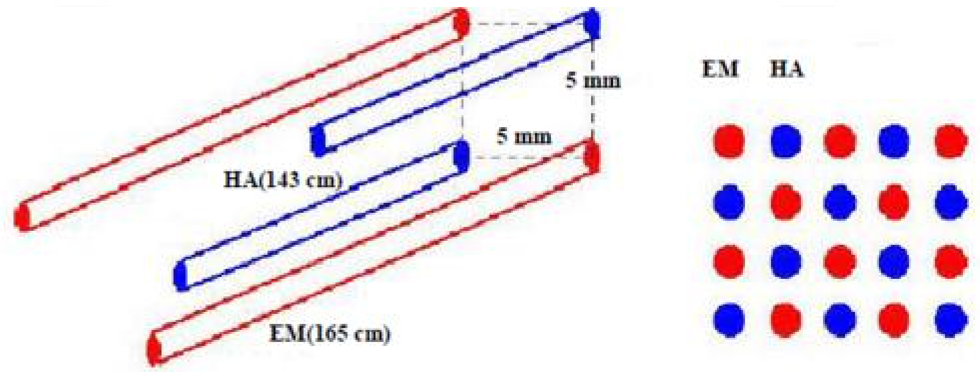

Figure 2.21. The layout of HF fibers in the absorber (Ozkurt, 2007).

Figure 2.22. The HF wedges.

The working principle of the HF calorimeter is based on Cherenkov radiation. Particles coming to HCAL interact with iron absorber and create secondary particles. These secondary particles interact again as long as their energies are enough to create new particles. This situation continues until particle energies fall below such energies that new particle creation stops. Formation of new particles in this manner is called development of a shower. The particles which interact electromagnetically create electromagnetic shower, while particles which interact strongly create hadronic shower. When charged shower particles velocities are above the Cherenkov threshold, they generate Cherenkov light in the fibers. The Cherenkov light which is produced by the relativistic components of the shower is transmitted to photo multipliers (PMTs) via quartz fibers. Long and short fibers are read out by separate photo multipliers. PMTs are electronic devices that convert light into electric current (CMS Note 2006/044).

2.2.3. Superconducting Magnet

One of the main goals of the CMS detector is to measure momenta of high energy particles and muons for new discoveries. To provide momentum measurement in high precision, a high magnetic field is needed. Therefore, the CMS decided to use a superconducting solenoid magnet which provides a 4T magnetic field (see Figure 2.23). The CMS superconducting magnet is designed to measure momenta of high energetic particles as precise as possible. The overall dimensions of the CMS magnet are a length of 12.5 m, a diameter of 6.3 m. Its weight is 12000 t. It is separated to five modules each with a length of 2.5 m. The CMS magnet is the largest in volume and the strongest in magnetic field along ever constructed magnets. It runs at –268.5 ^{o}C and it has a maximum energy of 2.6 GJ which can be stored in it. The solenoid magnet of CMS covers the tracking system and inner calorimeters. It is located in the center of the CMS and surrounded by the muon system. Also, the magnet provides mechanical support for the parts inside it. Parameters of the CMS magnet are summarized in Table 2.1 (http://cms.web.cern.ch/news/superconducting-magnet).

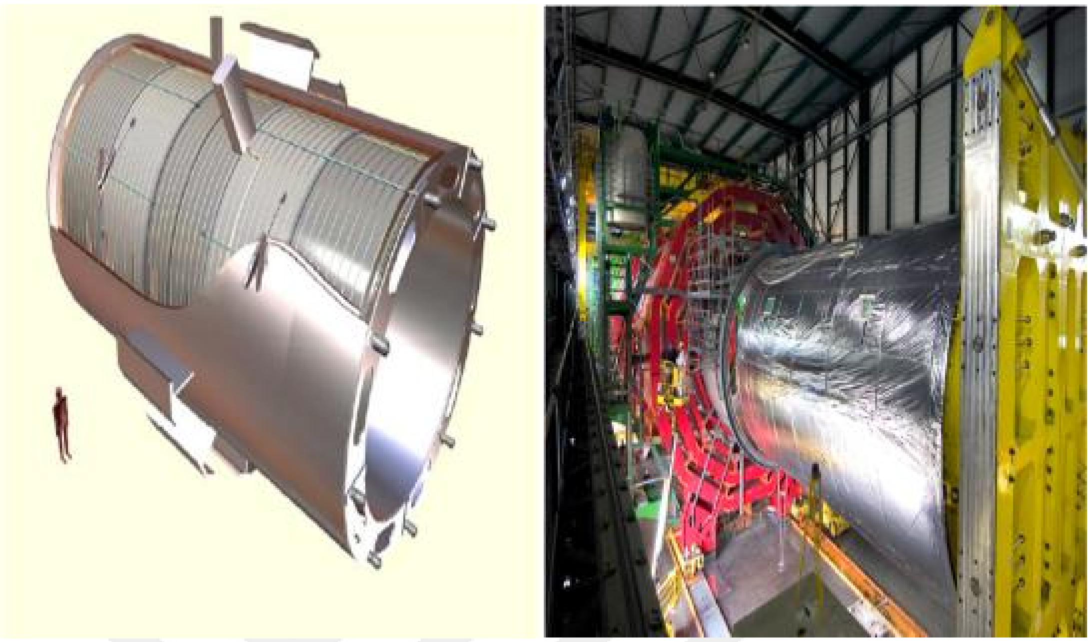

Figure 2.23. CMS superconducting magnet.

Table 2.1. Main parameters of the CMS magnet (CMS Collaboration, 2008, JINST 3 S08004).

Magnetic field	4 T
Inner bore	5.9 m
Length	12.9 m
Number of turns	2168
Current	19.14 kA
Stored energy	2.6 GJ
Hoop stress	64 atm

2.2.4. Muon System

The muon system is the largest and one of the most important components of the CMS. It is designed to determine muons and measure their momenta. When combined with the inner tracker system measurement of muon momenta becomes excellent. They are placed outside the CMS magnet and cover the pseudorapidity region of $|\eta| < 2.4$. Muons are fundamental particles with charge of $-e$ like electrons, but they are much heavier. They are minimum ionizing particles which can penetrate several meters of iron without interacting. Muons cannot be stopped by calorimeters and they do not generate electromagnetic showers. However, all other particles are stopped before reaching muon chambers. That is the reason to place muon chambers in the outer part of the CMS. The geometrical layout of the CMS muon system is shown in Figure 2.24. CMS uses three types of gaseous detectors for measurement of muons:

- Aluminum Drift Tubes (DT),
- Cathode Strip Chambers (CSC),
- Resistive Plate Chambers (RPC).

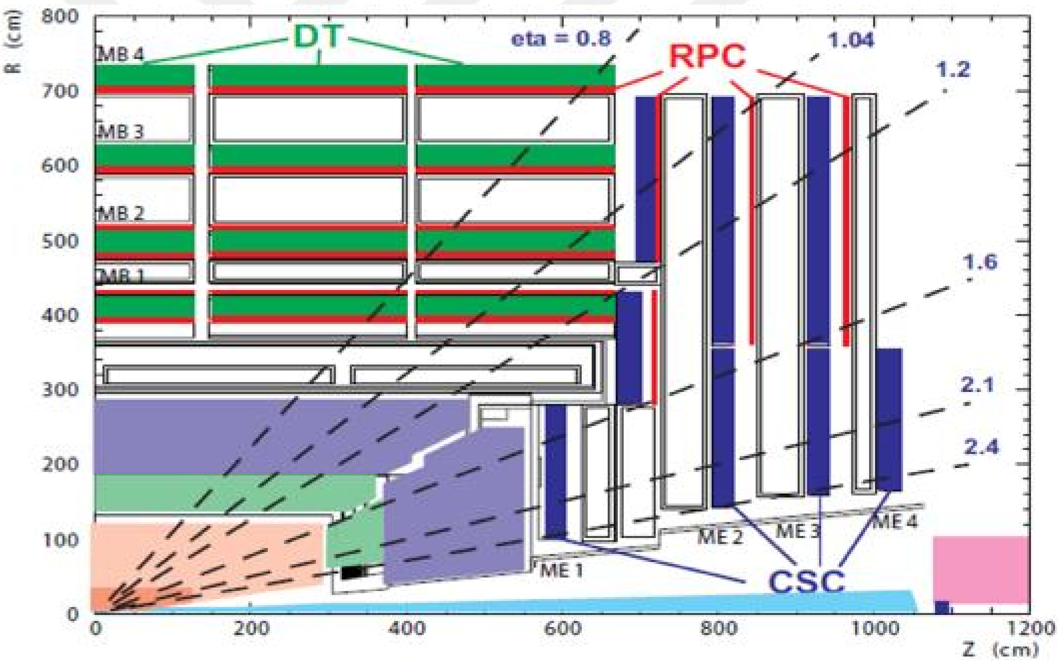

Figure 2.24. Overview of the CMS muon system (CMS TDR, 2006).

2.2.4.1. Muon Barrel System: Drift Tubes

The barrel drift tube chambers cover the pseudorapidity region of $|\eta| < 1.2$ and are used to measure tracks of muon particles at the barrel region. The muon barrel system composes of four concentric cylinders around the beam line as shown in Figure 2.25. Drift tubes are made of 4 cm wide tube and each tube contains wires which are inside a gas mixture (85% Ar, 15% CO_2). The length of wire in the chambers is around 2.4 m. Each DT chamber is composed of 12 aluminum layers called as super layer and each super layer contain 60 drift tubes which were organized at dimensions of 2 m × 2.5 m. The barrel muon system consists of four muon stations (MB1, MB2, MB3, MB4) which are placed at distance of 4.0 m, 4.9 m, 5.9 m and 7.0 m from the beam line respectively. The three inner cylinders have 60 drift chambers each. The outer cylinder has 70 drift chambers. About 172000 sensitive wires were used in this part of the detector. The Drift Tubes only placed in barrel part of the CMS (CMS Collaboration, 2008, JINST 3 S08004).

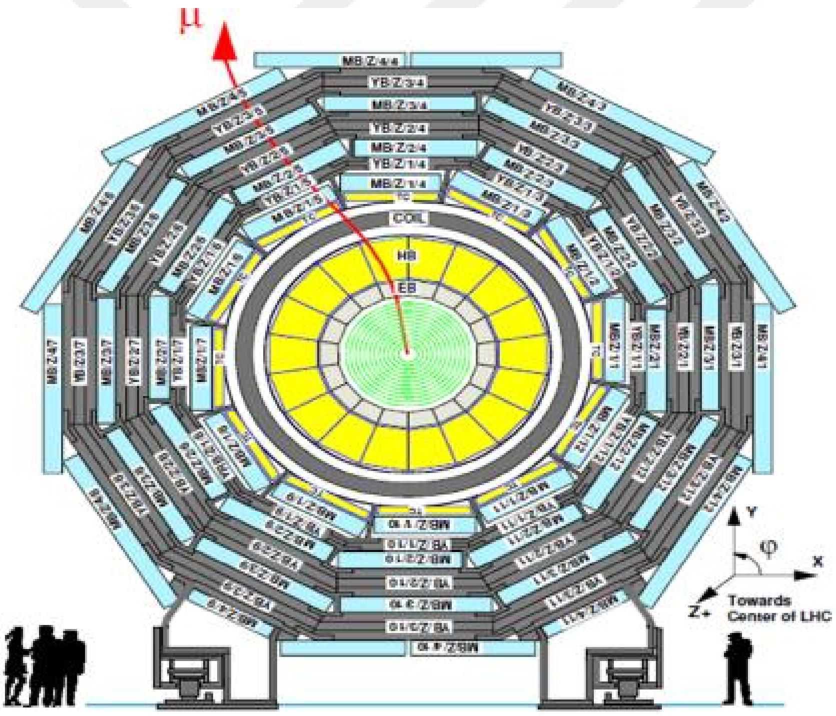

Figure 2.25. Layout of the CMS barrel muon DT chambers in one of the five wheels.

2.2.4.2. Muon Endcap System: Cathode Strip Chambers

The endcap muon system of CMS consists of 468 Cathode Strip Chambers (CSCs). The CSCs have fast response time and are radiation resistant. They are used only in the endcap region which have high particle flux and cover pseudorapidity region of $0.8 < |\eta| < 2.4$. Each muon endcap system consists of four stations labeled as ME1, ME2, ME3 and ME4. They are placed at increasing distances from the beam line respectively. These stations are built in disk geometry enclosing the solenoid magnet and placed perpendicularly to the beam direction. When muons pass through the chamber, they ionize gas atoms and produce an electron-ion pair. Ions are collected by the cathode and electrons are collected by the anode. Avalanche of electrons produces signal in the anode wire, while avalanche of ions in the cathode strips. In the CSCs strips and wires are placed perpendicular to each other in order to measure two coordinates. CSCs wires are spaced almost equally and it provides precise time and space resolution. Tracks of muons in the endcap region are measured with a high precision in this way. CSCs are shown in Figure 2.26 (CMS TDR, 2006).

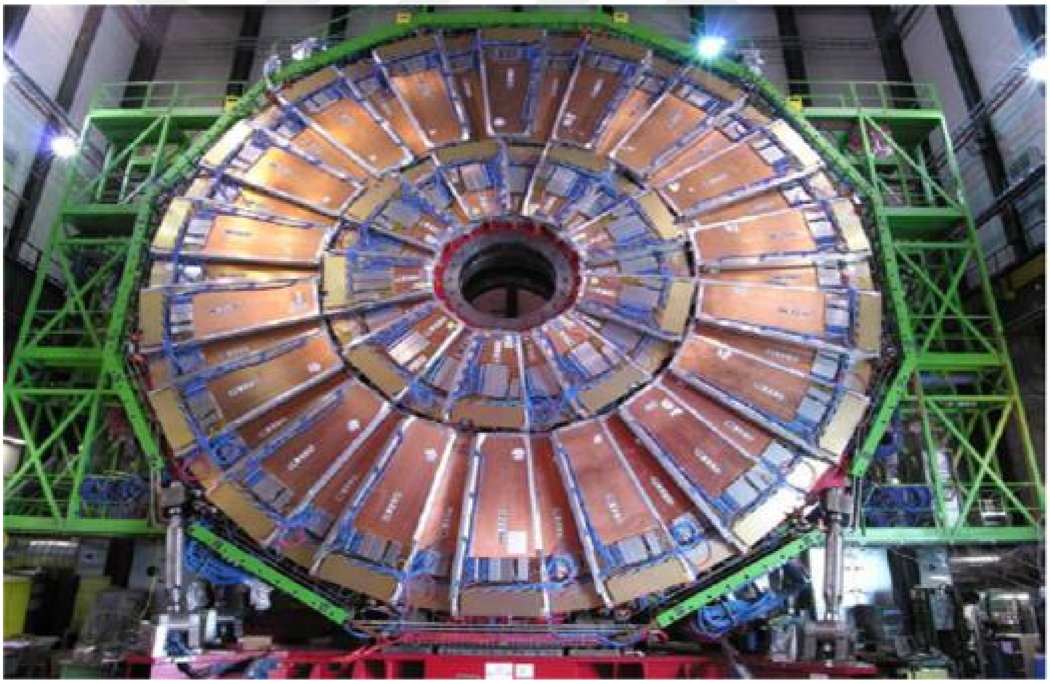

Figure 2.26. The muon endcap system (CMS Collaboration, 2008, JINST 3 S08004).

2.2.4.3. Resistive Plate Chambers

The Resistive Plate Chambers (RPCs) are gaseous parallel plate detectors. The RPCs are made of high resistivity plastic anode and cathode parallel plates and cover the pseudorapidity range of $|\eta| < 1.6$. The RPCs are located in both the barrel and endcap regions of muon system and used 610 RPCs in the muon system. The CMS RPCs are double gap chambers which have a width of 2 mm and operated in avalanche mode in order to provide good operation at high rates. They have a good time resolution and provide a very fast signal. That is why they are very important part of the trigger system. The location of RPCs is given by Figure 2.27 (CMS Collaboration, 2008, JINST 3 S08004).

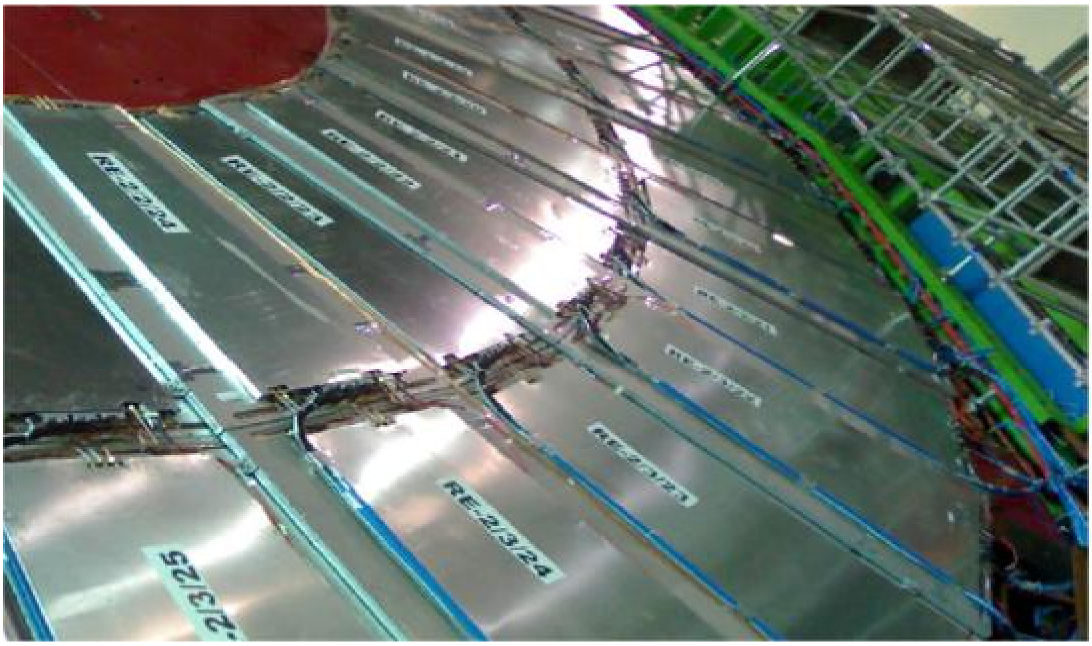

Figure 2.27. Resistive Plate Chambers of muon system in the CMS.

2.2.5. Trigger System

The p-p and heavy ion collisions in the LHC occur at high interaction rates. The crossing frequency of p-p collisions is 40 MHz which corresponds to a beam crossing interval of 25 ns. Approximately 20 p-p collisions occur at each crossing at the nominal design luminosity of 10^{34} cm^{-2} s^{-1}. When particles coming from interactions are detected by the detectors a large amount of data is generated at the LHC. The event size is about 1.5 MB for every p-p collisions. To collect this data is very hard and takes time. All events coming from a collision are not interesting physically and a drastic rate of reduction has to be achieved. Therefore, a trigger system is needed in order to select interesting physics events. CMS used a trigger system which has two levels. They are labeled as Level-1 (L1) and High Level Trigger (HLT) respectively.

2.2.5.1. Level-1 Trigger

The Level-1 trigger system is a hardware trigger and reduces the event rate from 40 MHz down to 100 kHz. It consists of custom-designed and largely programmable electronics. The L1 trigger decision is based on proto-objects; such as photons, electrons, muons and jets. The electronics of L1 trigger system is located at 90 m outside of the detector. The time interval to make decision for one bunch crossing is nearly 3.2 μs at L1. Events which are only accepted by L1 trigger system are processed by the HLT trigger system. The L1 trigger system is organized into three basic subsystems:

- L1 Calorimeter Trigger,
- L1 Muon Trigger,
- L1 Global Trigger.

The information from L1 Calorimeter Trigger and L1 Muon Trigger are transferred to L1 Global Trigger which makes the final accept-reject decision. L1 Muon Trigger includes information from RPC, CSC and DT. The architecture of the L1 trigger can be seen in Figure 2.28.

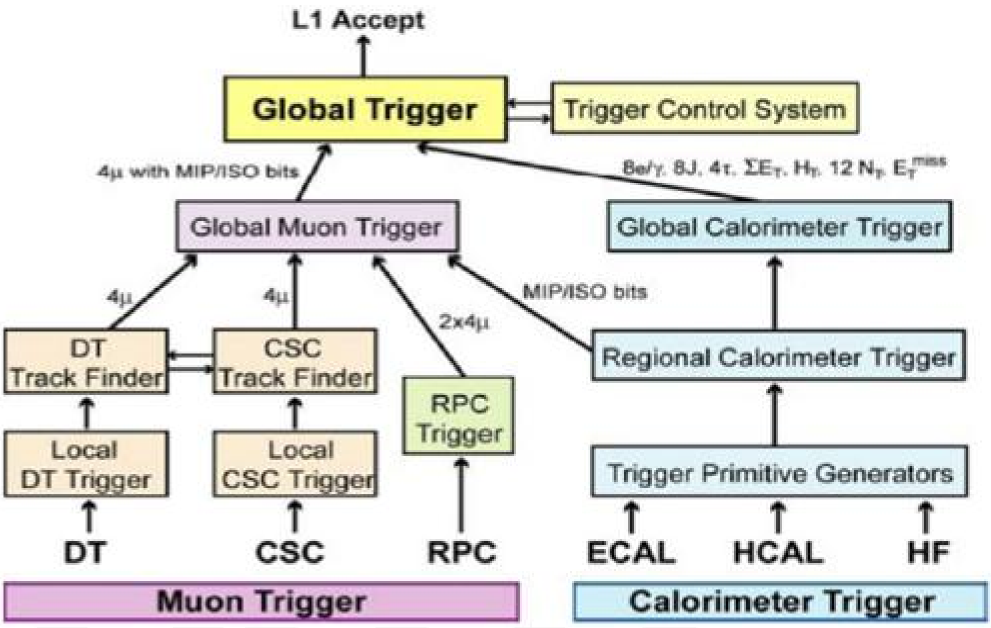

Figure 2.28. Architecture of the CMS Level-1 Trigger System.

2.2.5.2. High Level Trigger

The High Level Trigger system is software-based and has the task to further reduce the event rate from 100 kHz to 100 Hz. It reads all detector information from front-end electronics using zero suppression and data compression techniques in order to reduce size of event. Physics objects such as muons and jets are reconstructed in high precision and details when compared to L1 trigger. At this stage, information coming from inner tracker system is used in order to get better momentum resolution for charged particles. Given that the HLT is purely software-based, it could be developed according to a better understanding of the detector. All accepted events are forwarded to data quality monitoring. The information on the trigger decision is stored and is used to categorize and label events based on the physics goals.

3. ANALYSIS AND RESULTS

The primary goal of the CMS experiment is to discover new particles at the TeV energy scale using the proton-proton collisions by the Large Hadron Collider. This thesis includes some performance studies of HCAL which is a subdetector of the CMS.

A large number of cosmic data which are called Mid-Week Global Run (MWGR), Cosmic Run at Zero Tesla (CRUZET) and Cosmic Run at Four Tesla (CRAFT), have been taken between June 2014 and April 2015 by using various configurations. Many different studies by different analysis groups have been performed with the cosmic data. Various subsystems, including the tracking system, ECAL, HCAL and muon detectors, were operated to collect data with and without the magnetic field. During the cosmic muon data taking, different configurations of trigger systems, algorithms and datasets, have been used and a few million cosmic muons have been collected to control each HCAL sub-system in detail (CMS Collaboration, 2010, JINST 5 T03012).

In April 2015, the LHC beam delivered to CMS detector consisted of a single 450 GeV proton bunch. The LHC beam was steered into collimators located 150 m upstream in either direction from interaction point of the detector. Such events are referred to as “beam splash” events which are very useful to determine the timing information of the HCAL systems (CMS Collaboration, 2010, JINST 5 T03013).

In May 2015, the first proton-proton collisions were seen at center of mass energy of $\sqrt{s}$ = 13 TeV. In June 2015, magnet was on and CMS has taken p-p collision data at time intervals of 50 ns. Then some technical performance studies have been completed and p-p collision data were taken by the CMS at every 25 ns in August 2015. During the 13 TeV p-p collision, CMS recorded many collision events at the different configurations and algorithms to check the general performance of HCAL at the CMS.

3.1. Mid-Week Global Run Analysis

The components of the Hadronic Calorimeter (HB, HE, HO, HF) should have a good energy resolution. To achieve this goal, the measured energy and time parameters of all units of HCAL system should be controlled regularly. One of the methods used to do these controls is to benefit from global data which is recorded when there is no collision in the detector.

The MWGR that composed of the ten stages (MWGR1, 2, 3, 4, 5, 6, 7, 8, 9 and 10) were taken between 2 June 2014 and 30 January 2015 at different time and conditions, when the magnet was off. General status of HCAL was investigated in detail at each stage.

The MWGR analysis has been done by using minimum bias and cosmic datasets separately and the results coming from these datasets were compared. Minimum bias datasets contain minimum trigger conditions. Cosmic data will be described in detail in this chapter. The trigger chosen for the minimum bias dataset is L1_SingleJet16 trigger and for cosmic dataset is L1_SingleMuOpen trigger. Jet trigger is used in order to see abnormalities in jet events and to analyze problems coming from the jet algorithms. The muon trigger system is usually used to analyze events which proceeded from cosmic muon rays and to understand features of these muon events in detail.

At the global run data analysis, a lot of runs which were taken in different conditions (like trigger, pedestal…) and times were analyzed. The response of each HCAL components was examined using different datasets and triggers. Results of this analysis were compared for these components to decide if the trigger system is accurate or not.

Energy and time plots were obtained for each HCAL sub-system and their distributions have been investigated. Energy and time distributions of each HCAL component are shown in Figure 3.1 and Figure 3.2. HB, HE, HO energy and time distributions give information about energy and general time conditions of reconstructed hits in each HCAL component. *y*-axis indicates number of reconstructed hits in all of the histograms. *x*-axis shows energy scale (GeV) in energy histograms, time scale (ns) in time distributions.

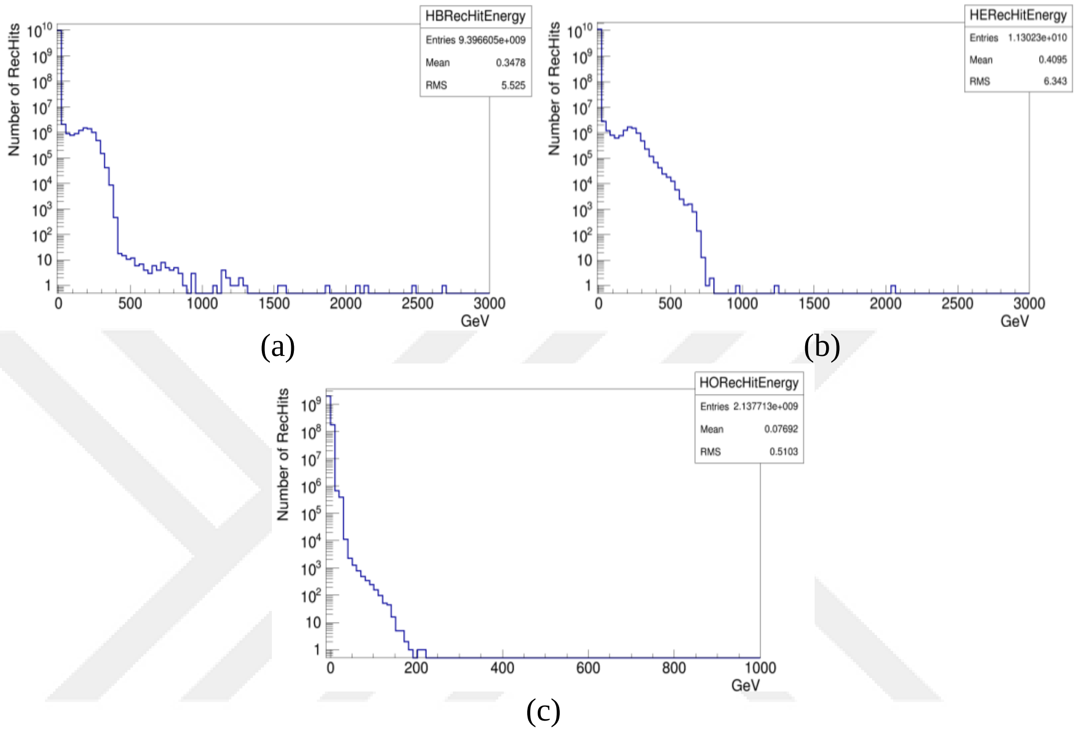

Figure 3.1. (a) HB, (b) HE, (c) HO rechit energy distributions.

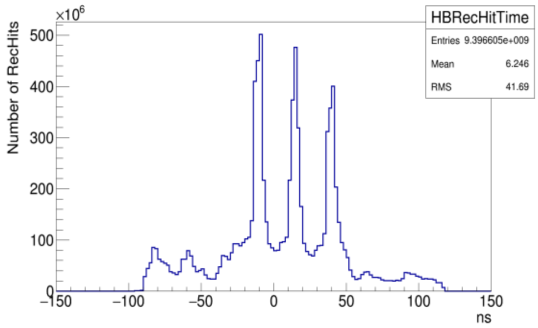

(a)

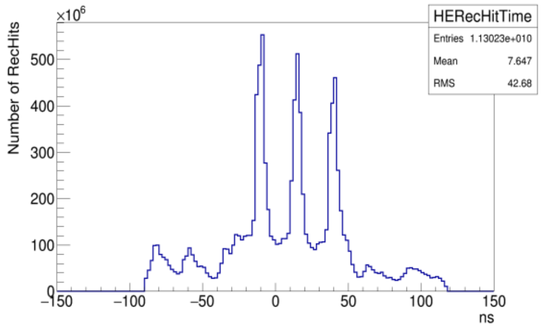

(b)

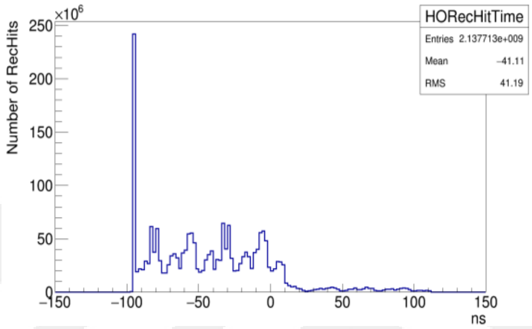

(c)

Figure 3.2. (a) HB, (b) HE, (c) HO rechit time distributions.

Furthermore, occupancy plots which indicate conditions of the rechits at each channels in HB, HE, HO were obtained to understand the problems. These occupancy plots are shown in Figure 3.3. x-axis represents ieta, y-axis represents iphi and z-scale (which is shown as a color) represents number of entries.

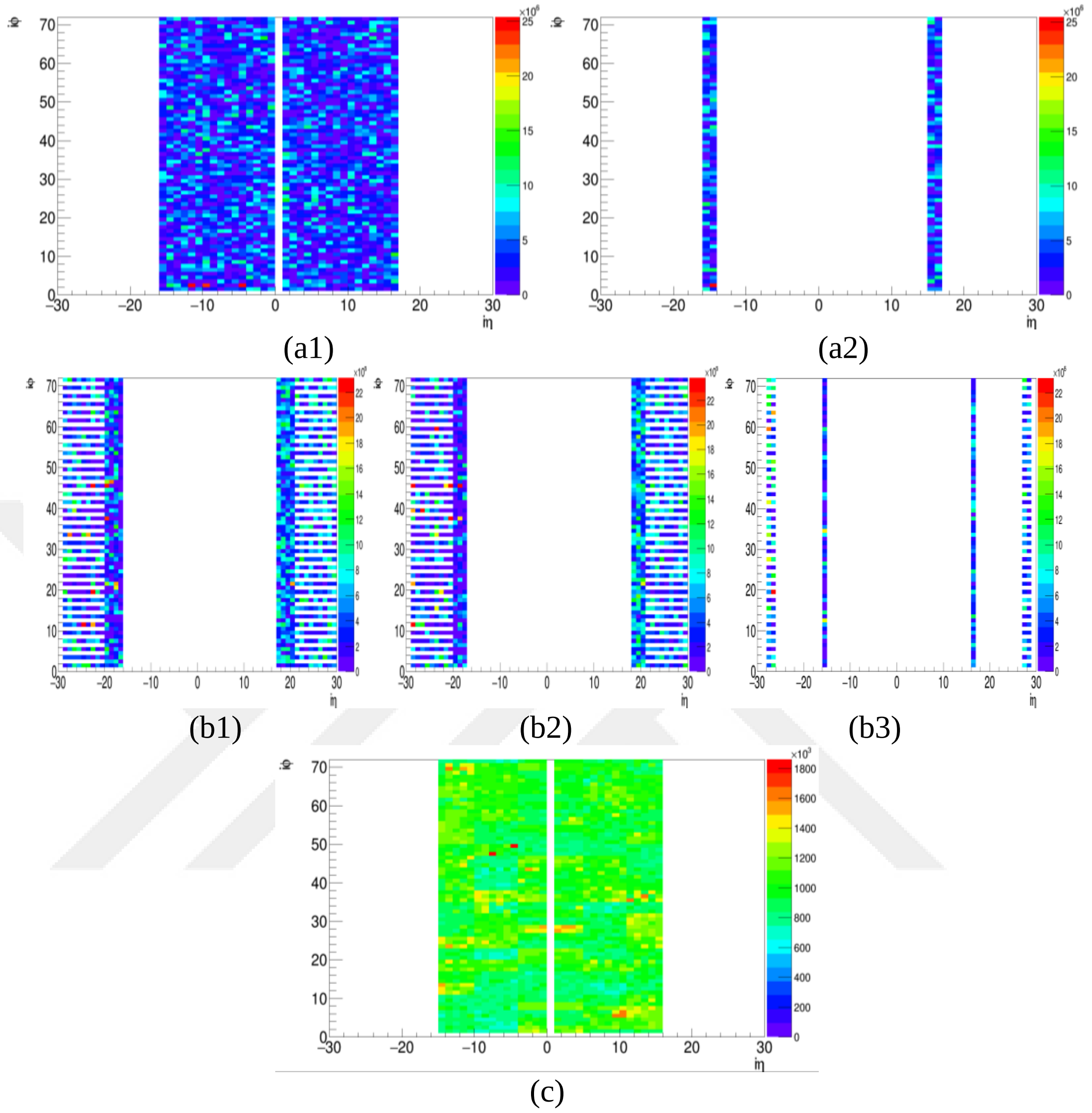

Figure 3.3. (a1) HB occupancy plot Depth1, (a2) Depth2, (b1) HE occupancy plot Depth1, (b2) Depth 2, (b3) Depth 3, (c) HO occupancy plot Depth4.

Energy and time information of each HCAL component could be different than others depending on the topology of HB, HE and HO calorimeters. Also, this topological effect can be seen at the occupancy plots which show the condition of rechits in each calorimeter channel. It can be clearly concluded that, MWGR analysis plays important role to determine the general performance of the HCAL.

3.2. Cosmic Run at Zero Tesla and Cosmic Run at Four Tesla Analysis

Cosmic rays are in close relation to the particle physics. Many particles, known as positron, muon, pion and kaon in particle physics, commonly were first discovered in the cosmic ray experiments. Energy of the ultra-high energetic cosmic rays which were observed in the air shower experiments is much higher than what LHC can provide.

Cosmic rays are known as high energetic particles which are continuously bombarding the earth and coming from astronomical objects. From the view point of a high energy physicist, if high energetic particles are thought as a beam and our world as a target, this situation can be served as a "fixed target experiment", as shown in Figure 3.4.

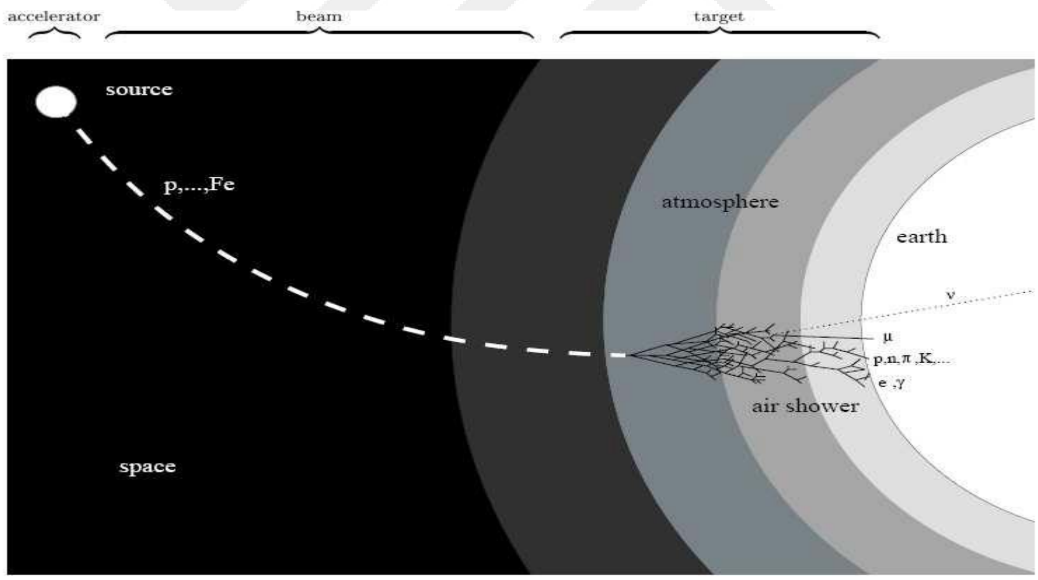

Figure 3.4. The schematic view of the cosmic fixed target experiment.

The primary particles and their secondary particles, e.g., muons, interact with the atmosphere of the earth. Thus, when these particles arrive to the earth surface they interact with the CMS detector and are detected. Cosmic rays coming from the atmosphere hit the detector at random times and random directions. Therefore, cosmic pedestal data should be separated from the collision data in order to take good data.

While waiting for the 13 TeV collision data (proton-proton), the CMS detector takes cosmic muon ray data in different time periods in order to prepare the detector for collision. Cosmic muon ray data were recorded by the CMS detector in two different conditions; magnet off (CRUZET) and magnet on (CRAFT). The main goal of the CRUZET and CRAFT analysis is to make controls of general energy and time resolution of each sub-detector of HCAL. Also, the response of each HCAL sub-system is measured thanks to these analyses. During the CRUZET and CRAFT, CMS detector collected approximately 300 million cosmic muon events.

CRUZET and CRAFT data were taken between 9 February and 30 March 2015. At the CRUZET and CRAFT analysis, many runs having different qualities and features were taken in specific dates and times. In order to keep energy and time resolution of HCAL and its components in good condition they should be controlled regularly in terms of energy and time parameters. One of the methods used to do these controls is to benefit from cosmic ray muon data which is recorded when there is no collision in the detector.

While CRUZET and CRAFT analysis were performed, two different datasets and trigger systems had been used. They are called minimum bias and cosmic datasets and jet trigger and cosmic muon trigger respectively. In the CRUZET and CRAFT analysis, when minimum bias dataset was used, jet trigger is chosen. Jet trigger generally is used in order to understand whether there are any abnormal situations in the physics events which contain jets. Cosmic muon trigger generally is used in order to see conditions arising from cosmic ray muon events. During the CRUZET and CRAFT analysis, energy and time distributions of each HCAL components (HB, HE and HO) were investigated and compared for cosmic and minimum bias datasets separately. HB, HE and HO rechit energy and rechit time distributions were obtained using cosmic dataset. Their results are shown in Figure 3.5 and Figure 3.6 respectively. In these figures, *x*-axis shows energy scale (GeV) at energy distributions and time scale (ns) at time distributions. Also in all of the histograms *y*-axis shows number of rechits. When analysis results of CRUZET and CRAFT are compared, it can be seen that they have some differences which could be due to magnetic field effect.

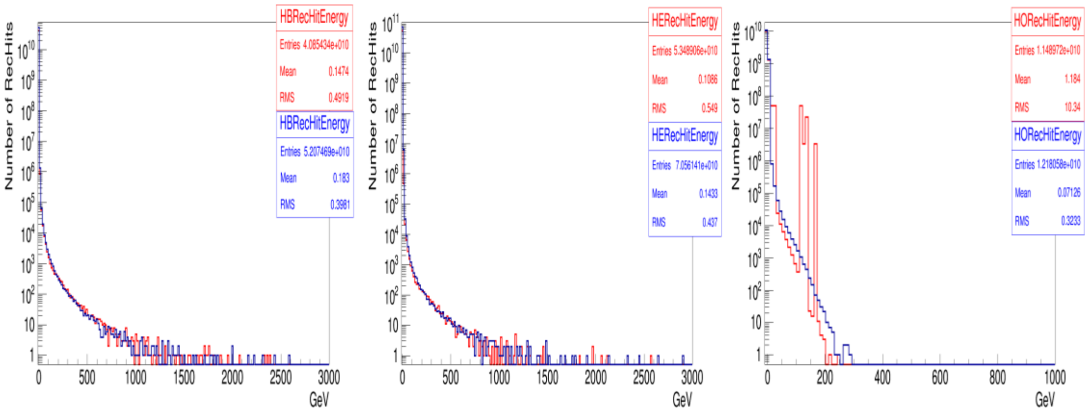

Figure 3.5. CRUZET (represented with red line) and CRAFT (represented with blue line) rechit energy distributions for cosmic dataset.

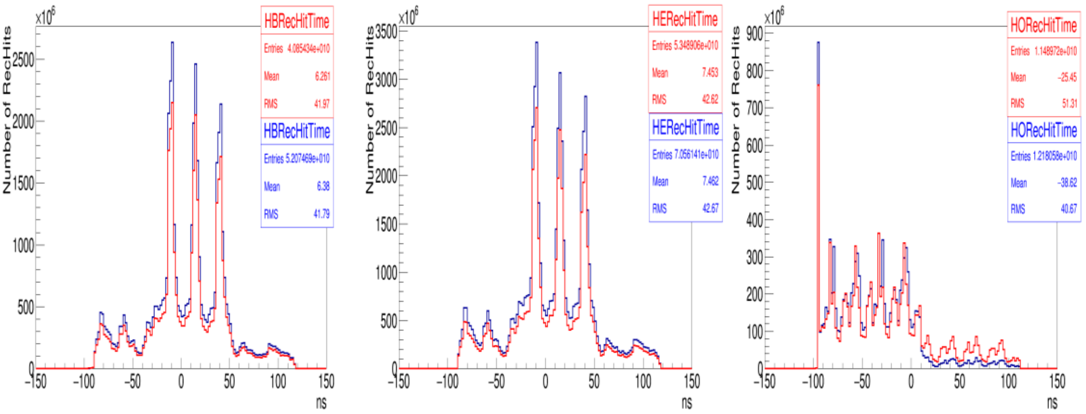

(b)

Figure 3.6. CRUZET (represented with red line) and CRAFT (represented with blue line) rechit time distributions for cosmic dataset.

In addition HB, HE and HO energy and time distributions have been obtained for minimum bias dataset for CRUZET and CRAFT by using same method with cosmic dataset. HB, HE and HO rechit energy distributions can be seen in Figure 3.7 and rechit time distributions in Figure 3.8. As can be seen from plots, CRUZET and CRAFT results have some differences. These differences can be arising from the behaviors of particles in each sub-system depending on magnetic field.

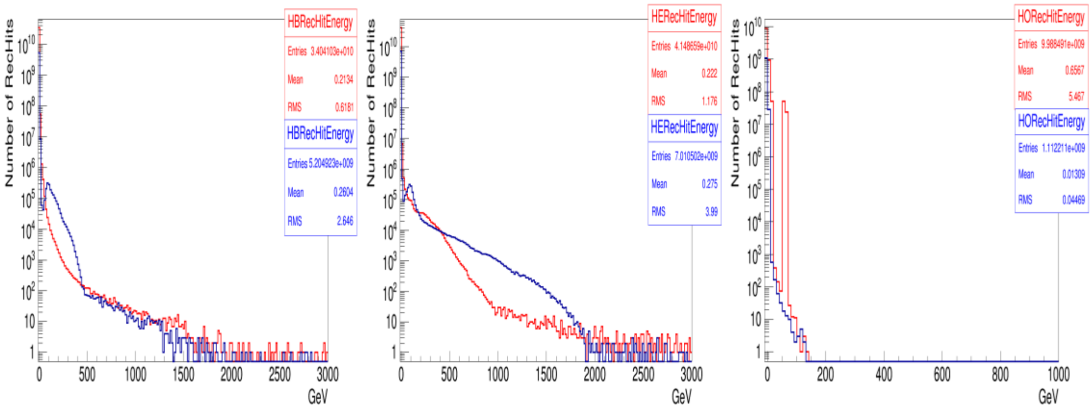

Figure 3.7. CRUZET (represented with red line) and CRAFT (represented with blue line) rechit energy distributions for minimum bias dataset.

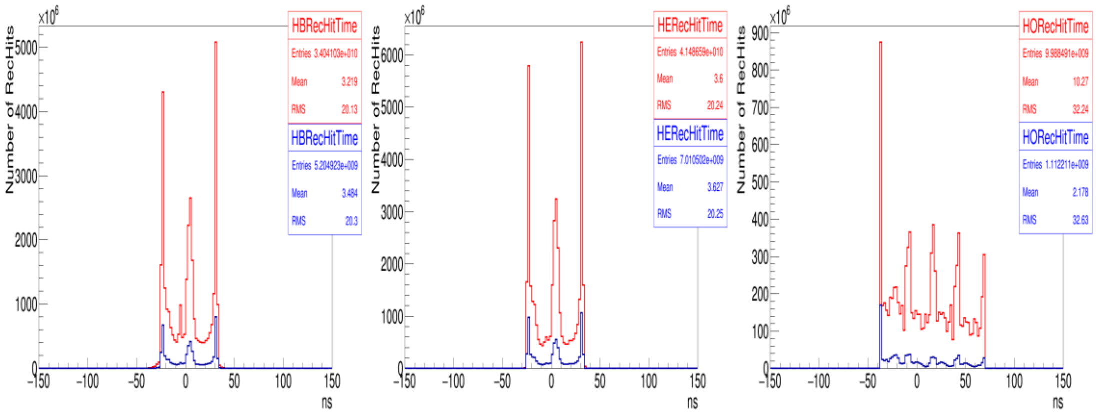

(b)

Figure 3.8. CRUZET (represented with red line) and CRAFT (represented with blue line) rechit time distributions for minimum bias dataset.

During these analyses, noisy/dead channels had been investigated by using occupancy plots. These plots indicate conditions of rechits at each channel of HCAL sub-systems. Conditions of HB, HE and HO in the CRUZET analysis are shown in Figure 3.9. In all of the occupancy plots *x*-axis indicates ieta, *y*-axis indicates iphi and *z*-scale represents number of entries. According to HB, HE and HO occupancy plots, there were some problematic channels (red points) at each depth. These channels have high energetic rechits and these red points which are seen for some channels arise from those rechits.

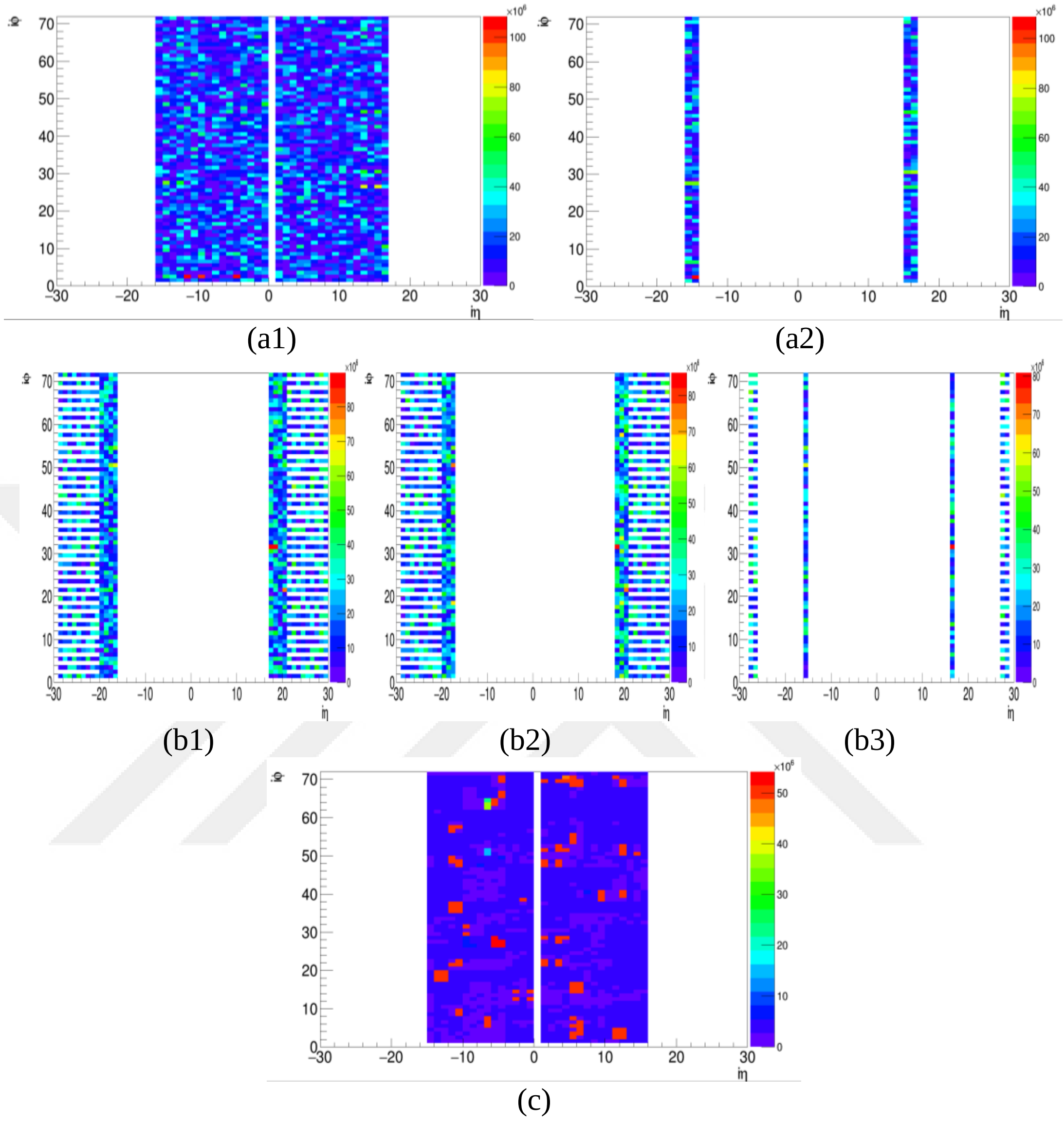

Figure 3.9. (a1) HB occupancy plot Depth1, (a2) Depth2, (b1) HE occupancy plot Depth1, (b2) Depth2, (b3) Depth3, (c) HO occupancy plot Depth4 for CRUZET.

HB, HE and HO occupancy plots were also obtained for CRAFT analysis by using the same method with CRUZET. These results can be seen in Figure 3.10. Some channels seen as red points are because of high energetic rechits. These channels were determined and analyzed specifically in order to see the cause of problems in these channels.

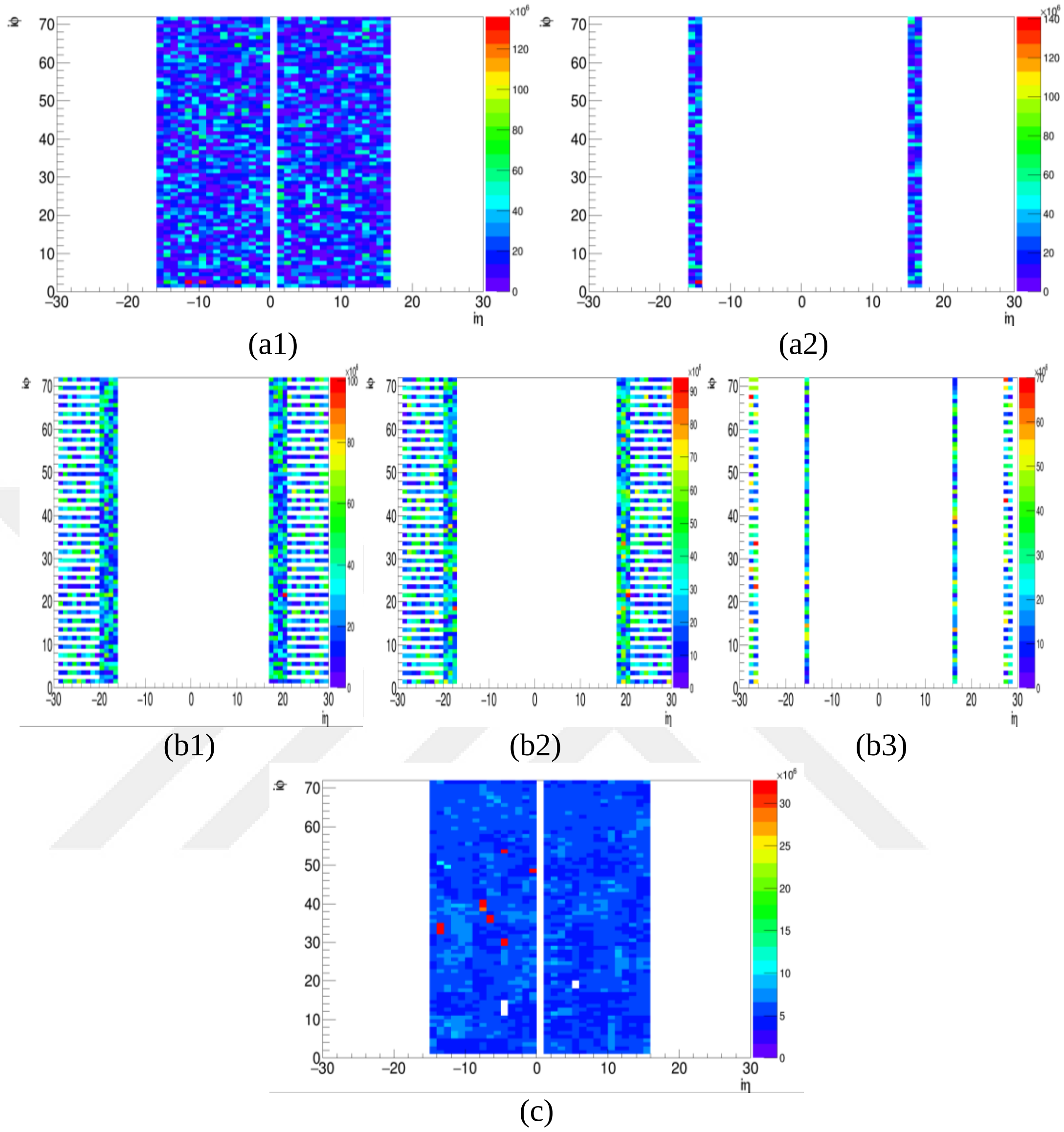

Figure 3.10. (a1) HB occupancy plot Depth1, (a2) Depth2, (b1) HE occupancy plot Depth1, (b2) Depth2, (b3) Depth3, (c) HO occupancy plot Depth4 for CRAFT.

According to the obtained results, it is decided that some of the problems at these channels have arisen from pedestal of the detector and high energetic rechits. Problematic channels suffered from the pedestal were reported to detector performance groups as a list. This list can be found in the followings tables.

Table 3.1. HB Bad Channels from CRUZET.

ieta	-4	-9	-11	-14	-15	-16	-14	-15	16	17
iphi	2	2	2	2	54	54	27	27	30	30

Table 3.2. HE Bad Channels from CRUZET.

ieta	20	-15	-16	-15	-16	16	17
iphi	21	50	50	54	54	31	31

Table 3.3. HB Bad Channels from CRAFT.

ieta	2	7	-4	-11	-9	-14
iphi	8	8	2	2	2	2
Depth	1	1	1	1	1	2

Table 3.4. HE Bad Channels from CRAFT.

ieta	26	27	26	-18	29	16	20	20	-26	27	-17	19
iphi	67	3	67	3	49	54	21	21	19	17	18	20
Depth	1	1	2	2	2	3	1	2	3	3	2	2

Table 3.5. HO Bad Channels from CRAFT.

ieta	-13	-4	-6	-7	-7	-4	-7	-1	10	11
iphi	34	29	35	38	40	30	39	48	38	27
Depth	4	4	4	4	4	4	4	4	4	4

To conclude; during the CRUZET and CRAFT analysis, much data which were taken at different times and having different qualities were analyzed in order to be more precise. General condition of the HCAL was tried to be understood with these analyses. Also a lot of studies were done to improve the performance of the detector. Cosmic ray data taken as CRUZET and CRAFT provided an opportunity to test magnetic field effect in each HCAL component.

3.3. Beam Splash Analysis

Beam Splash data which is important in terms of performance analysis of the CMS detector was taken between 5 and 11 April 2015 at 450 GeV. Proton beam was steered into collimators located at 150 m upstream in either direction of the CMS's interaction point and detector exposed to dense particles flow. Such events are called as "Beam Splash" events.

The Beam Splash analysis allows us to understand the behavior of HCAL components which were exposed to dense particle flow. During this analysis two runs were analyzed and their results investigated in detail. Analyzed runs are 239754 and 239895; also minimum bias dataset was used. At this analysis, six events were recorded for run 239754 but only four events which are available for timing was taken. Furthermore, run 239895 were analyzed at two section referred to as Beam 1 and Beam 2. Twenty six events that belong to Beam 1 and thirty one events belonging to Beam 2 were studied at this analysis.

In the Beam Splash analysis energy graphs which belong to HB and HE sub-calorimeters were obtained in order to understand the energies of rechits at three different depths for two runs separately. HBHE energy histograms for these runs can be seen in Figure 3.11. In all of the HBHE energy histograms, *x*-axis shows ieta value, *y*-axis shows iphi value and *z* scale represents the energy.

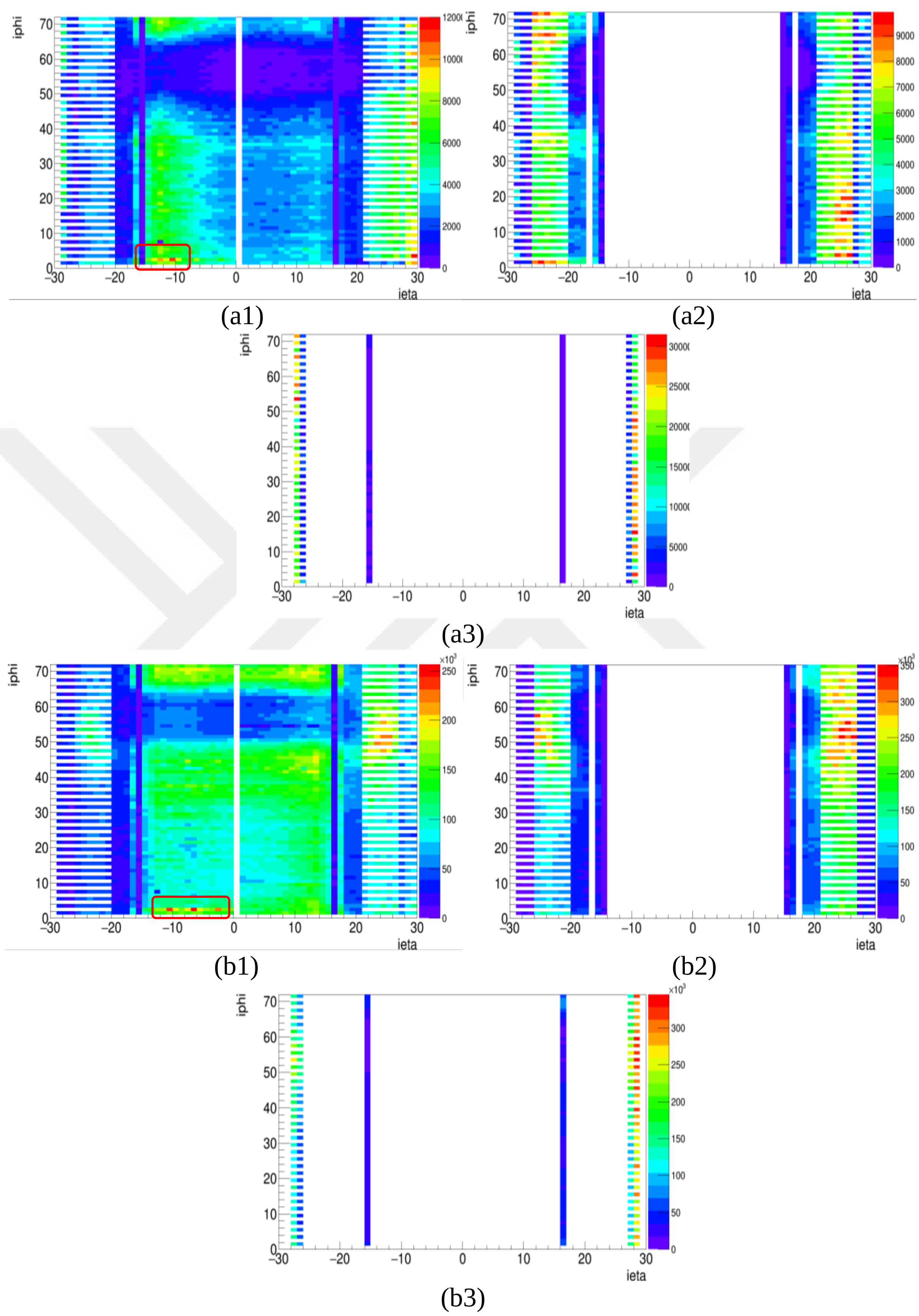

Figure 3.11. (a1) HBHE energy histograms Depth1, (a2) Depth2, (a3) Depth3 for splash run 239754, (b1) HBHE energy histograms Depth1, (b2) Depth2, (b3) Depth3 for splash run 239895.

These plots show that, most of the individual channels in HB and HE are stable but HBM iphi 2 channels were unstable. Also it is seen that, HBM iphi 2 channels have a different behavior. From the point of view of detector performance group, this problem is coming from the pedestal. To understand this problem in detail, some ratio plots were obtained according to Eq.3.1 and 3.2 for these two runs separately. The energy deposited in iphi 2 which is thought to be problematic has been compared to the energy deposited in neighboring iphis (1 and 3) which behave more stable. The ratio value should be close to one. If it is close to one, then there is no problem. But as can be seen from Figure 3.1, the ratio is not close to one for iphi 2. Big deviation from one indicates a problem for this channel.

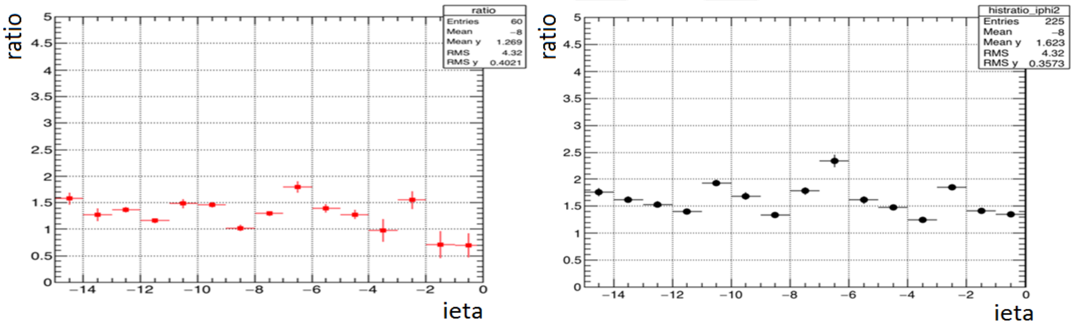

(a) (b)

Figure 3.12. Ratio plots for HBM iphi 2 channel, (a) splash run 239754, (b) splash run 239895.

The same ratio plots were made for iphi4 which is a stable channel using the same runs to see the condition of this channel. The ratio plots of iphi4 can be seen in Figure 3.13. When Figure 3.13 is compared to Figure 3.12 it can be seen that iphi 2 channel has a problem. Ratio distribution of iphi 4 indicates a more stable distribution around 1, as it was expected. This problem was reported to performance groups.

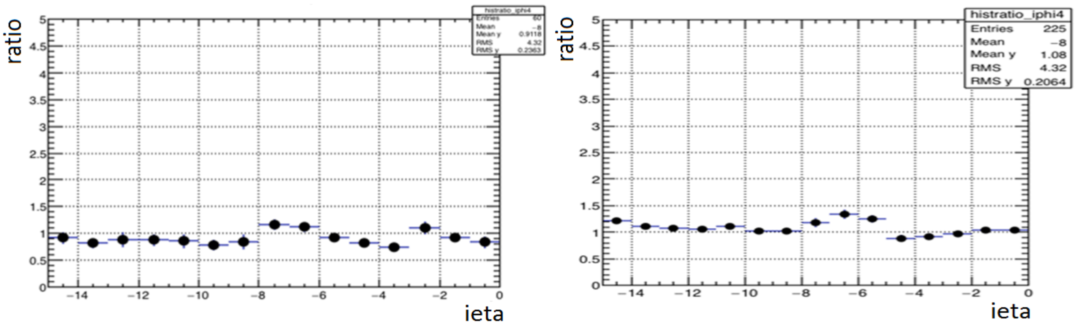

(a) (b)

Figure 3.13. Ratio plots for HBM iphi 4 channel, (a) splash run 239754, (b) splash run 239895.

$$ratio = \frac{energy(iphi2)}{[(energy(iphi1)+energy(iphi3)]/2}. \quad (3.1)$$

$$ratio = \frac{energy(iphi4)}{[(energy(iphi3)+energy(iphi5)]/2}. \quad (3.2)$$

At the Beam Splash, since the CMS detector is exposed to dense particle flow, QIE cards were saturated. These saturated hits can be selected or eliminated by the application of a saturation filter. At this analysis, to understand the conditions of rechits after saturation is very important. When the saturation filter was applied, only saturated rechits are taken. Nevertheless, when the saturation filter was not applied, all rechits are taken.

To understand conditions of saturated rechits which are located in each HCAL component is very important in terms of the productivity of the Beam Splash analysis. Therefore, performance analysis of each HCAL system should be done in high precision. Results from saturated rechits for HB and HE sub-systems are shown in Figure 3.14 and 3.15.

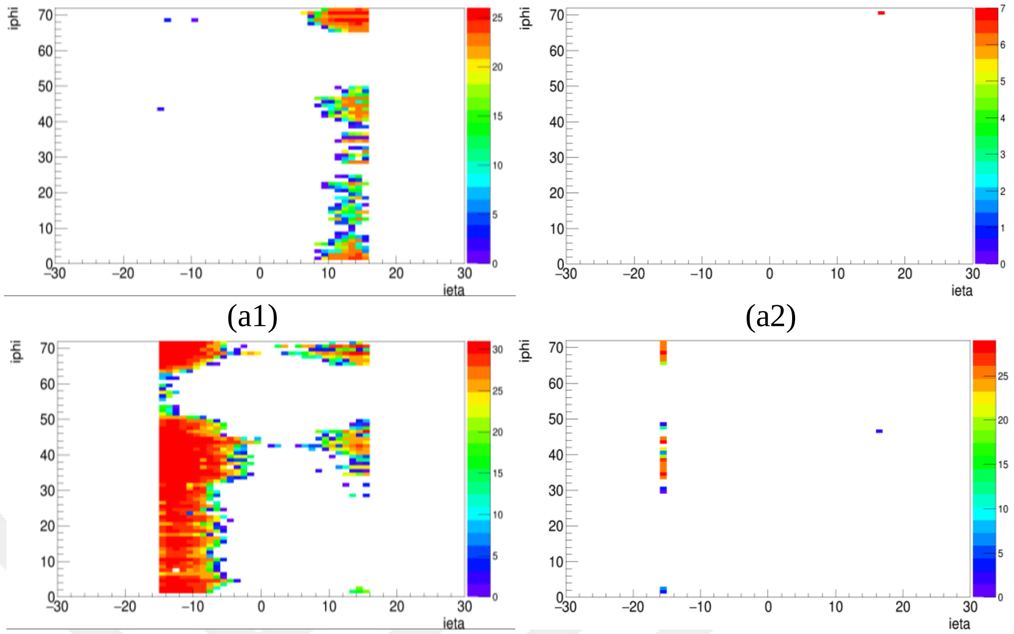

(a1) (a2)

(b1) (b2)

Figure 3.14. (a1) HB occupancy plot Depth1, (a2) Depth2 for Beam 1, (b1) HB occupancy plot Depth1, (b2) Depth2 for Beam 2.

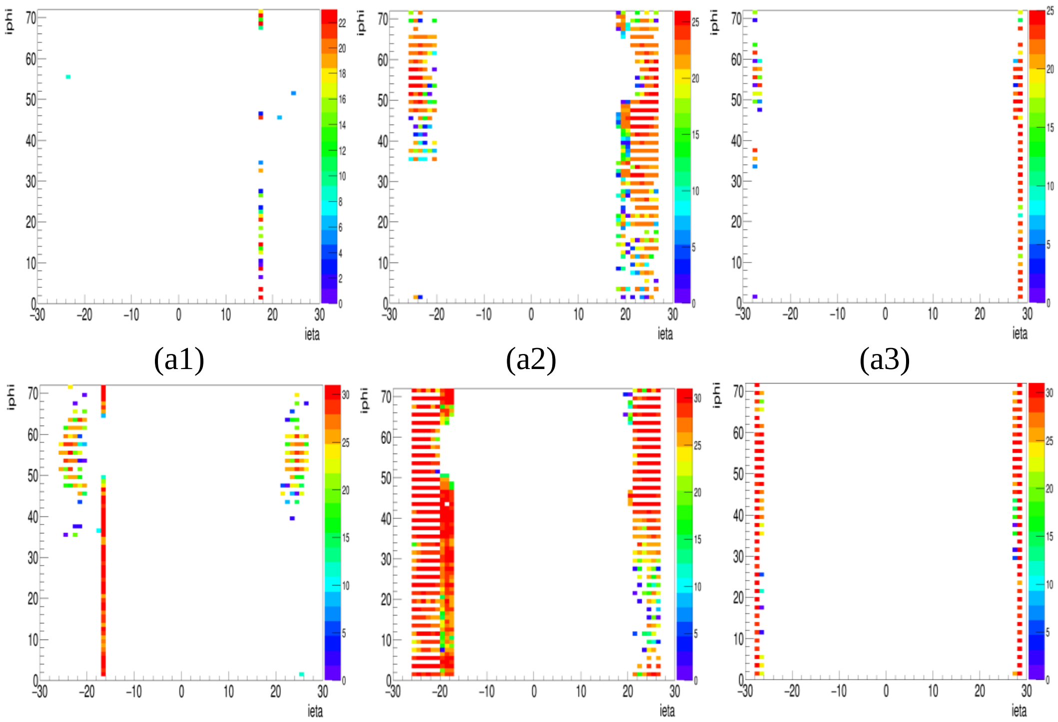

(a1) (a2) (a3)

(b1) (b2) (b3)

Figure 3.15. (a1) HE occupancy plot Depth1, (a2) Depth2, (a3) Depth3 for Beam 1, (b1) HE occupancy plot Depth1, (b2) Depth2, (b3) Depth3 for Beam 2.

In addition, energy plots which indicated general conditions of HB, HE, HO and HF calorimeter with and without saturation filter are shown in Figure 3.16. For all distributions *x*-axis indicates energy scale (GeV) and *y*-axis indicates number of reconstructed hits. Also, red line represents reconstructed hits energies without saturation filter, blue line with saturation filter. Number of rechits which are unsaturated is less than number of rechits which are normal.

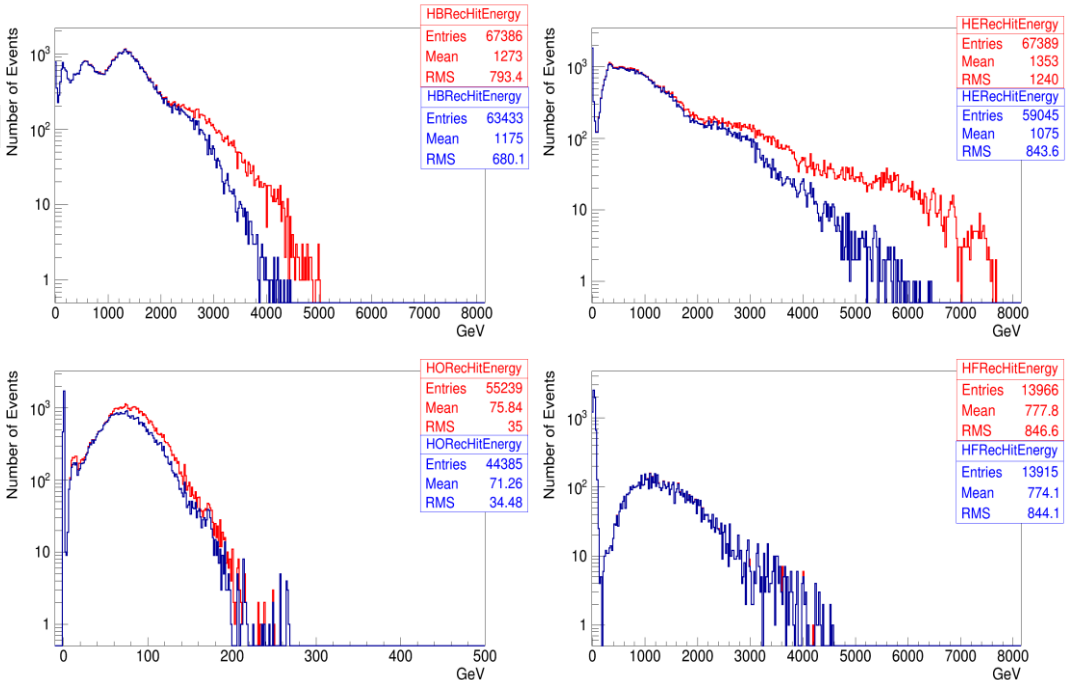

Figure 3.16. HB, HE, HO, HF unsaturated and all rechit energy distributions.

Beam Splash analysis provided an understanding of the response of the CMS detector against dense particle flow and obtained information about HCAL performance. The software studies were completed by Beam Splash analysis and CMS detector was prepared for 13 TeV collision data.

3.4. Performance of the CMS Calorimeter System with 13 TeV proton-proton Collision Data

After the two-year technical stop, on 21 May 2015 the first p-p collision event were observed at the LHC at a center of mass energy of $\sqrt{s}$ = 13 TeV. During the technical break, calibration studies of each part of the CMS detector were done by using different techniques. In this period some part of the detector were renovated and detector was tested in order to achieve a high efficiency.

In this study, performance analysis of each component of HCAL was performed using p-p collision data in detail. Different data that are taken in specific date and time periods are used at this analysis. On 6 June 2015, the LHC took collision data when magnet was off. In addition, the CMS detector recorded collision data at every 50 ns. After that, CMS detector recorded collision data at every 25 ns when the magnet was on (3.8T). The normal operating capability of the CMS detector was arranged to take data every 25 ns by doing some studies that reduced the pile-up effect.

During the 13 TeV collision data taking, numerous runs were analyzed in order to understand general condition of HCAL and see the changes at the calorimeter for each data. Moreover, analysis was continued through some important plots for general performance analysis process of HCAL.

The Express Physics dataset was used at the 13 TeV collision data analysis. This dataset was taken at four different time periods, called as 2015A, 2015B, 2015C, 2015D. Each period represents a different stage. For example, when magnet off, the 2015A was taken, when magnet on, the 2015B was taken respectively. The 2015C data was taken in 25 ns period. Also, when the detector works in stable condition, the 2015D data was taken. Thus, energy and time distributions of each HCAL component were investigated with the help of physics data taken at the each period. Energy and time distributions for each dataset can be seen in Figure 3.17 to 3.24. In all of rechit energy distributions *x*-axis shows energy scale (GeV), *y*-axis shows number of reconstructed hits and in all of rechit time distributions *x*-axis shows time scale (ns), *y*-axis shows number of reconstructed hits. Rechit energy and time distributions were obtained for 2015A, 2015B, 2015C and 2015D datasets separately to see differences between these datasets in detail.

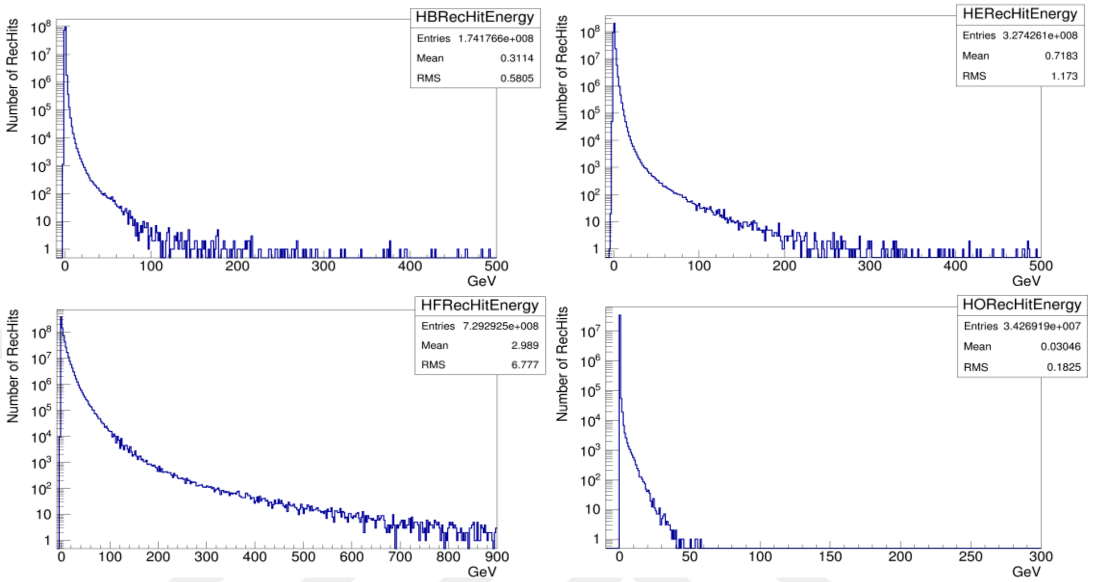

Figure 3.17. HB, HE, HF and HO rechit energy distributions (2015A dataset, 0T, 13 TeV).

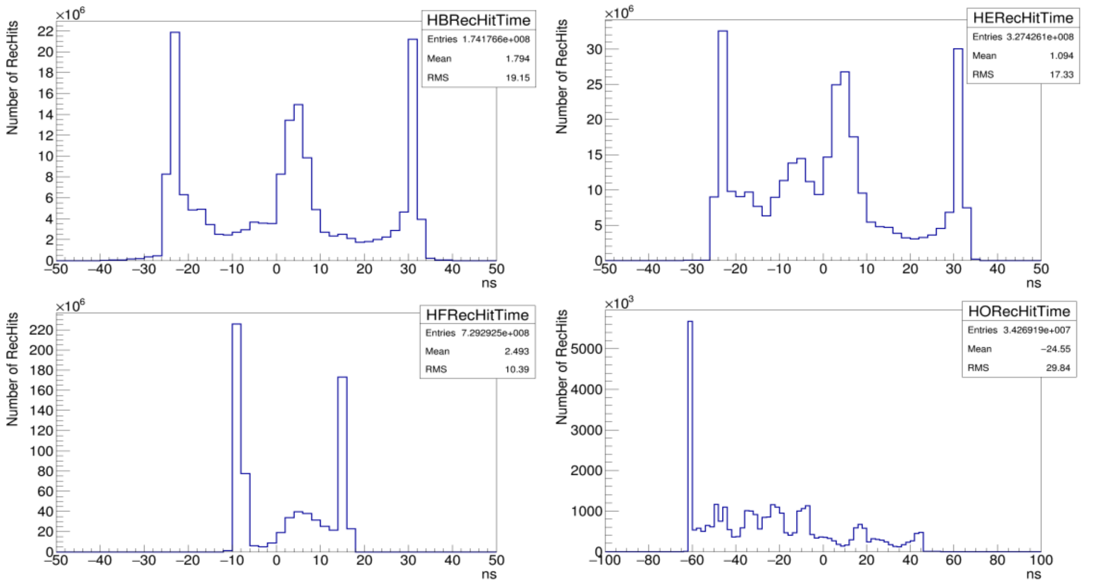

Figure 3.18. HB, HE, HF and HO rechit time distributions (2015A dataset, 0T, 13 TeV).

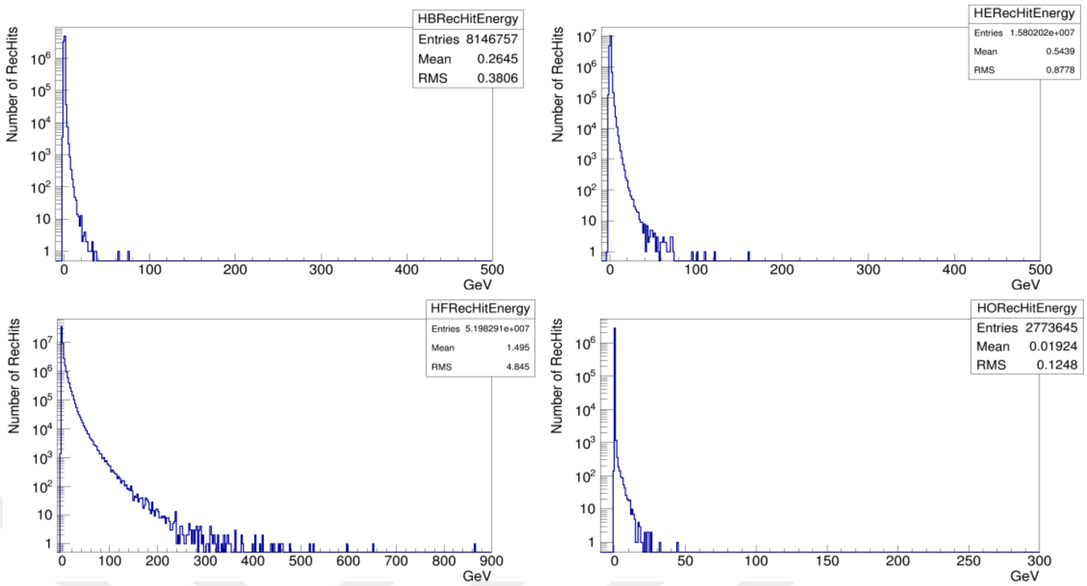

Figure 3.19. HB, HE, HF and HO rechit energy distributions (2015B dataset, 3.8T, 13 TeV).

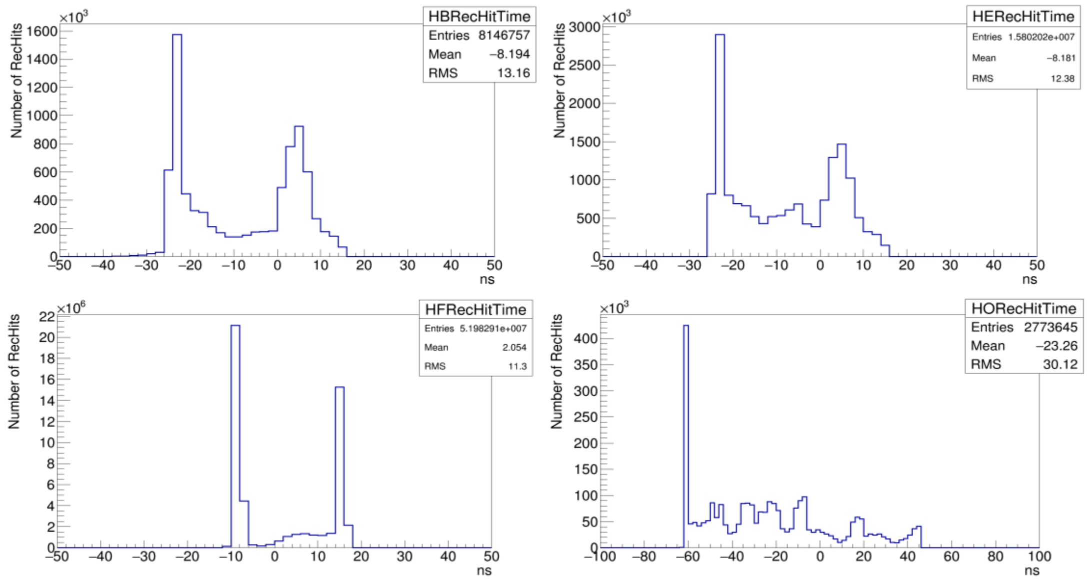

Figure 3.20. HB, HE, HF and HO rechit time distributions (2015B dataset, 3.8T, 13 TeV).

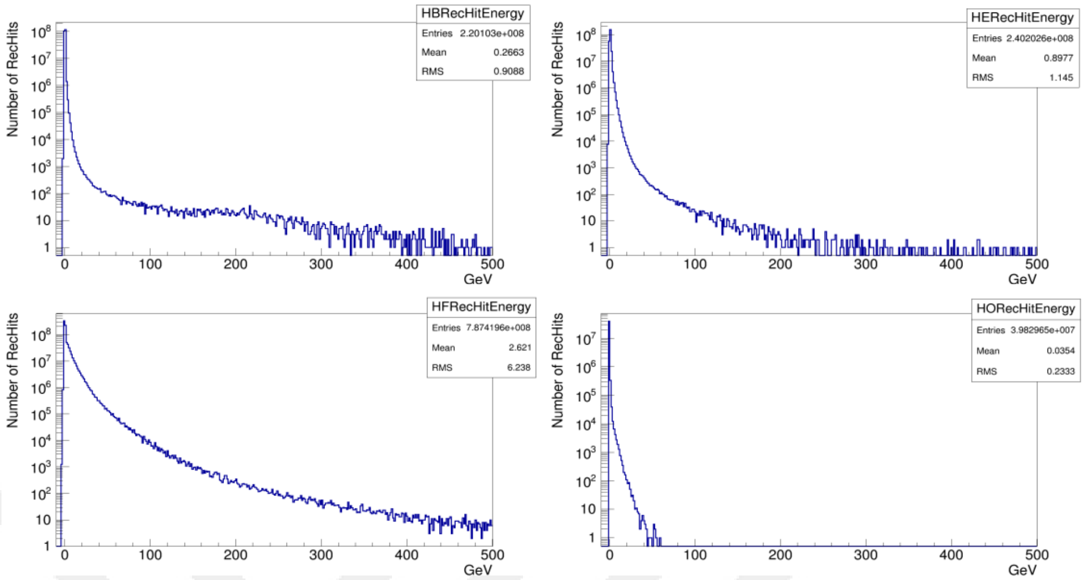

Figure 3.21. HB, HE, HF and HO rechit energy distributions (2015C dataset, 3.8T, 13 TeV).

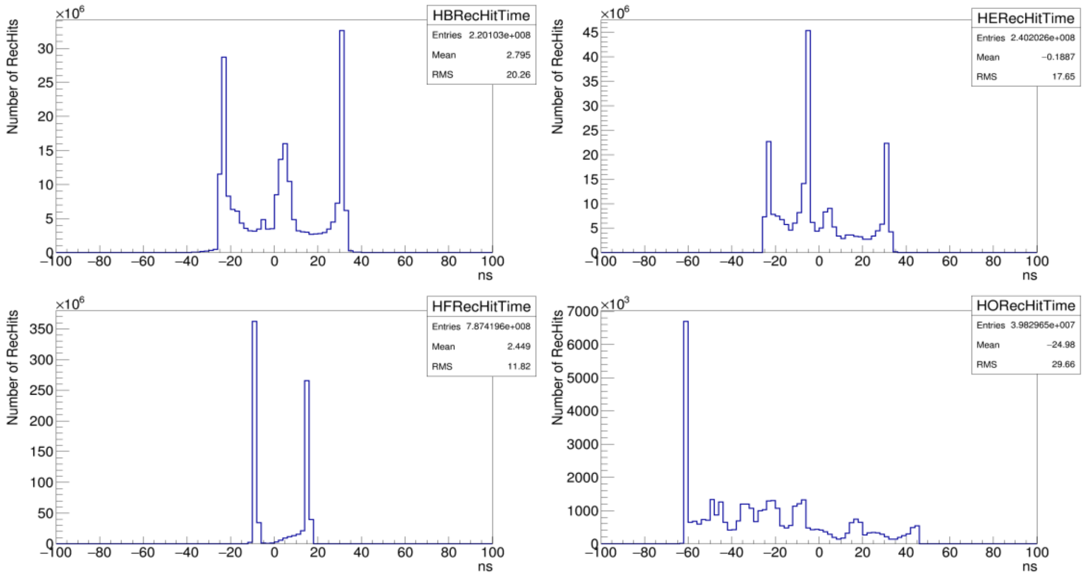

Figure 3.22. HB, HE, HF and HO rechit time distributions (2015C dataset, 3.8T, 13 TeV).

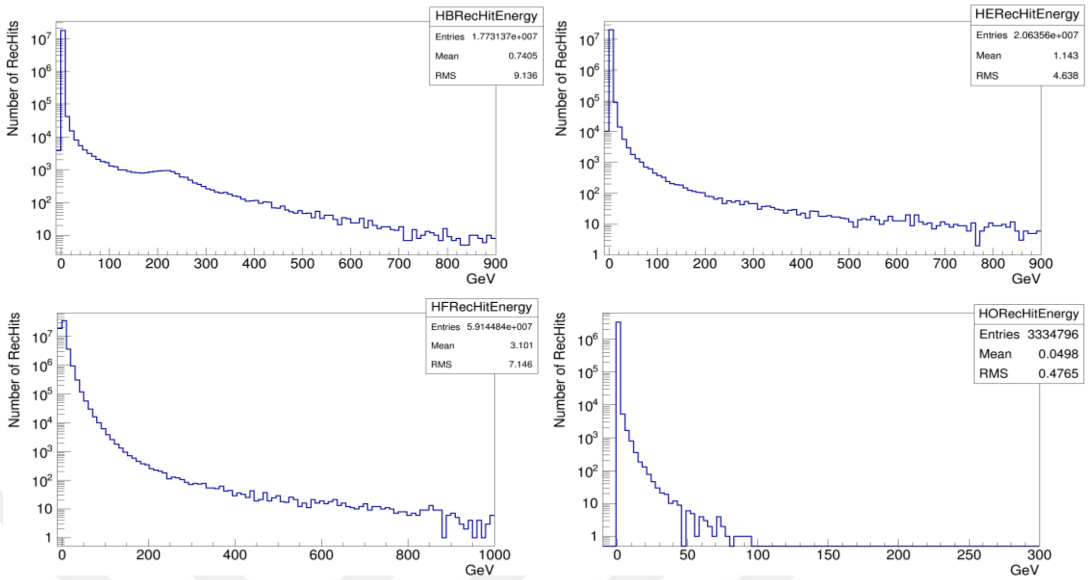

Figure 3.23. HB, HE, HF and HO rechit energy distributions (2015D dataset, 3.8T, 13 TeV).

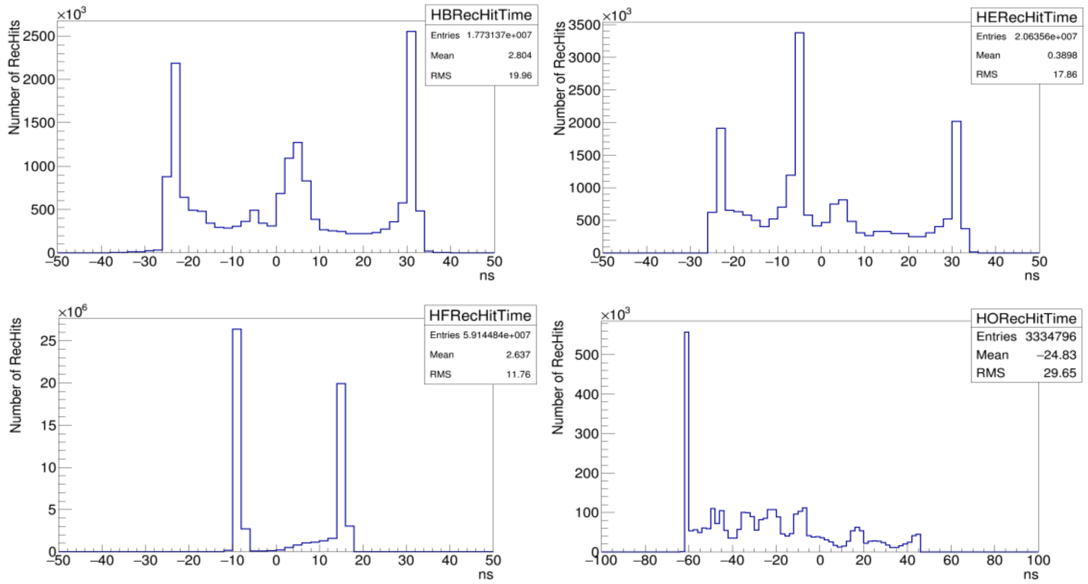

(b)

Figure 3.24. HB, HE, HO and HF rechit time distributions (2015D dataset, 3.8T, 13 TeV).

During this analysis, some abnormal conditions were seen on HF time plots. With other information from the detector performance groups it is decided that these abnormal conditions at the HF time plots is coming from the reconstruction method.

During the 13 TeV collision data analysis, numerous data were analyzed by using different datasets and conditions in detail. Problems in this analysis were reported to detector performance groups. According to received information from these groups, problems were fixed and analysis completed for all datasets (2015A,B,C,D).

4. CONCLUSIONS

MWGR, Cosmic Muon, Beam Splash and p-p Collision Data were taken by CMS depending on the LHC program during 2015. The purpose of this study is to control the general condition of HCAL using these data and to look the central (HB, HE and HO) and forward (HF) regions of HCAL in detail. Thus, energy and time stability of all channels in HCAL sub-systems are determined in order to keep the performance of the calorimeter in high level.

In the first part of this study the global run (MWGR) data were used. During this analysis, different parameters and methods were used. The global run data were taken at specific times at ten stages, while all sub-systems of the CMS were working. All these data were used to check the problematic channels of all sub-systems of HCAL. These tests are very important in terms of reliability of the detector performance. At the end of the MWGR analysis, the performance analysis of HCAL was done successfully by using the global run data.

As a second part of this analysis, CRUZET and CRAFT data were used to benefit from cosmic muon ray data in order to check the energy and time parameters of HCAL system regularly. The cosmic muon rays hit various regions of the CMS detector and create signals. To control whether the CMS detector works efficiently, those signals were used. Like MWGR analysis, a lot of cosmic rays data which have different features were recorded at the specific time range in the CRUZET and CRAFT period. The energy and time stability of HB, HE and HO calorimeters were investigated by using these data. Two different trigger systems called as jet and muon trigger were used for CRUZET and CRAFT analyses and results from them were compared precisely. According to analysis results, number of events from cosmic muon data is higher than jet data. During these analyses, it was also seen that most of the HCAL channels were working properly, but some of them are problematic. Especially in some HCAL channels number of rechits is too big. Problematic HCAL channels are given for HCAL subsystem in the Table 3.1, 3.2, 3.3, 3.4 and 3.5 in the Analysis and Results chapter. These problems were coming from the pedestal and were eliminated by applying different energy cuts.

At the third part of this study, the beam splash data were used. During the beam splash data taking, the CMS detector was exposed to a dense particle flow. Thus, response of each sub-system of the CMS was investigated by using these data. The beam splash analysis is especially very important to test the performance of the HCAL system before the p-p collision. During the beam splash analysis, an unstable behavior of one channel (HB minus iphi 2) was found. This channel was compared with other channels which are more stable and were analyzed in detail. On the other hand, various filters were used in order to investigate the general condition of each channel. Because of the dense particle flow, some regions in each HCAL sub-system were saturated. These saturated channels were determined by using a saturation filter and these channels also were reported to the performance groups. The beam splash data analysis provided an opportunity to determine the response of CMS detector against dense particle flow. More information about these types of studies can be found at this link: https://twiki.cern.ch/twiki/bin/viewauth/CMS/HCALSplash2015.

The last part of this study is 2015 p-p collision data analysis. The problems (unstable channels) which were seen at the splash data analysis, were corrected before the collision data analysis. At the collision data analysis, energy and time stabilities of HB, HE, HO and HF calorimeters were investigated using the Express Physics dataset. This dataset was taken at four different time periods and called as 2015A, 2015B, 2015C, 2015D. According to the obtained results from collision data analysis, the channels of HCAL system were shown to be in a more stable condition.

REFERENCES

CERN Brochure, 2009. https://cds.cern.ch/record/1165534/files/CERN-Brochure-2009-003-Eng.pdf.

CERN Brochure, 2009. https://cds.cern.ch/record/1183425/files/CERN-Brochure-2009-006-Eng.pdf.

CERN Brochure, 2009. https://cds.cern.ch/record/1194057/files/CERN-Brochure-2009-007-Eng.pdf.

CERN Brochure, 2010. https://cds.cern.ch/record/1324123/files/CERN-Brochure-2010-007-Eng.pdf.

CERN Brochure, 2012. https://cds.cern.ch/record/1485019/files/CERN-Brochure-2012-004-Eng.pdf.

CMS Collaboration, 2006. "Detector Performance and Software", CMS Physics, Technical Design Report, Volume 1, CERN-LHCC 2006-001, http://cds.cern.ch/record/922757/files/lhcc-2006-001.pdf.

CMS Collaboration, 2006. "Physics Performance", CMS Physics, Technical Design Report, Volume 2, CERN-LHCC 2006-021, http://cds.cern.ch/record/942733/files/lhcc-2006-021.pdf.

CMS Collaboration, 2008. "The CMS experiment at the CERN LHC", The CERN Large Hadron Collider: Accelerator and Experiments, 122 p., http://iopscience.iop.org/1748-0221/3/08/S08004/pdf/1748-0021_3_08_S08004.pdf.

CMS Collaboration, 2010. "Commissioning of the CMS experiment and the cosmic run four tesla: Commissioning of the CMS Experiment with Cosmic Rays, http://iopscience.iop.org/article/10.1088/1748-0221/5/03/T03001/pdf.

CMS Collaboration, 2010. "Performance of CMS hadron calorimeter timing and synchronization using test beam, cosmic ray and LHC beam data", CMS Paper, FERMILAB-PUB-10-156-CMS, https://inspirehep.net/record/837888/files/fermilab-pub-10-156-cms.pdf.

CMS Collaboration, 2010. "Performance of the CMS Hadron Calorimeter with Cosmic Ray Muons and LHC Beam Data", CMS Paper, CMS PAPER CFT-09-009, https://arxiv.org/pdf/0911.4991.pdf.

CMS Collaboration, 2011. "Technical Proposal for The Upgrade of The CMS Detector Through 2020", CMS UG-TP-1, https://cds.cern.ch/record/1355706/files/LHCC-P-004.pdf.

CMS Collaboration, 2013. "Observation of a new boson at a mass of 125 GeV with the CMS experiment at the LHC", CMS-HIG-12-028; CERN-PH-EP-2012-220, http://arxiv.org/pdf/1207.7235v2.pdf.

CMS HCAL Collaboration, 2006. "Design, Performance and Calibration of CMS Hadron-Barrel Calorimeter Wedges", CMS Note, CMS NOTE 2006/138, http://cds.cern.ch/record/1049915/files/NOTE2006_138.pdf.

CMS HCAL Collaboration, 2006. "Design, Performance and Calibration of CMS Forward Calorimeter Wedges", CMS Note, CMS NOTE 2006/044.

CMS HCAL Collaboration, 2008. "Design, Performance and Calibration of CMS Hadron Endcap Calorimeters", CMS Note, CMS NOTE 2008/010, http://cds.cern.ch/record/1103003/files/NOTE2008_010.pdf.

CMS HCAL Collaboration, 2008. "Design, Performance and Calibration of CMS Hadron-Outer Calorimeter", CMS Note, CMS NOTE 2008/020, https://inspirehep.net/record/802051/files/NOTE2008_020.pdf.

FOCARDI, E., 2011. "Status of the CMS detector", Conference Report, CMS CR-2011/214, TIPP 2011, http://cds.cern.ch/record/1395445/files/CR2011_214.pdf.

HAGOPIAN, V., 2009. "The Performance of the CMS Hadron Calorimeter with Cosmic Muons", Conference Report, CMS CR-2009/303, ICATPP09, https://cds.cern.ch/record/1358805/files/CR2009_303.pdf.

J. Beringer et al., "2012 Review of Particle Physics-Gauge and Higgs Bosons", Physical Review D 86: 1, 2012.

K.A. Olive et al., 2014. "Review of Particle Physics", (Particle Data Group), Chin. Phys. C, 38, 090001.

https://en.wikipedia.org/wiki/Standard_Model
http://en.wikipedia.org/wiki/Higgs_boson
https://home.cern/about/experiments/alice
https://home.cern/about/experiments/atlas
https://home.cern/about/experiments/lhcb
https://home.cern/about/experiments/lhcf
https://home.cern/about/experiments/totem
http://aliceinfo.cern.ch/Public/en/Chapter3/Chap3Collaboration-en.html
https://lhcb-public.web.cern.ch/lhcb-public/en/Collaboration/Collaboration-en.html
http://atlas.cern/discover/collaboration
http://hep.fi.infn.it/LHCf/
http://cms.web.cern.ch/content/cms-collaboration

CURRICULUM VITAE

Merve was born on February 8, 1988, in Adana, Turkey. She finished her high school education in Adana, 2005. She received her Bachelor's degree in Physics in 2013 from Cukurova University. She started the master degree in High Energy Physics in Cukurova University in 2014. She participated to experimental studies between 15 July and 15 September 2014, 1 April and 1 September 2015, 1 May and 1 July 2016 at CERN.